

1 Dynamics of Variable Dusk-Dawn Flow Associated with Magnetotail 2 Current Sheet Flapping

3
4 James H. Lane¹, Adrian Grocott¹, Nathan A. Case¹, Maria-Theresia Walach¹

5
6 ¹ Department of Physics, Lancaster University, Lancaster, UK

7
8 Correspondence to: James Lane (j.lane@lancaster.ac.uk)

9 10 11 Abstract

12 We present Cluster spacecraft observations from 12 October 2006 of convective plasma
13 flows in the Earth's magnetotail. Earthward flow bursts with a dawnward $v_{\perp y}$ component,
14 observed by Cluster 1 (C1), are inconsistent with the duskward flow that might be expected
15 at the pre-midnight location of the spacecraft. Previous observations have suggested that
16 the dusk-dawn sense of the flow can be governed by the Interplanetary Magnetic Field
17 (IMF) B_y conditions, with the related 'untwisting hypothesis' of magnetotail dynamics
18 commonly invoked to explain this dependence, in terms of a large-scale magnetospheric
19 asymmetry. In the current study, observations of the upstream solar wind conditions from
20 OMNI, magnetic field observations by Cluster, and ionospheric convection data using
21 SuperDARN, indicate a large-scale magnetospheric morphology consistent with positive IMF
22 B_y penetration into the magnetotail. At the pre-midnight location of Cluster, however, the
23 dawnward flow observed below the neutral sheet by C1 could only be explained by the
24 untwisting hypothesis in a negative IMF B_y scenario. The Cluster magnetic field data also
25 reveal a flapping of the magnetotail current sheet; a phenomenon known to influence dusk-
26 dawn flow. Results from the curlometer analysis technique suggest that the dusk-dawn
27 sense of the $\mathbf{J} \times \mathbf{B}$ force was consistent with localised kinks in the magnetic field and the
28 flapping associated with the transient perturbations to the dusk-dawn flow observed by C1.
29 We therefore suggest that the flapping overcame the dusk-dawn sense of the large-scale
30 convection which we would expect to have been net duskward in this case. We conclude
31 that invocation of the untwisting hypothesis may be inappropriate when interpreting

32 intervals of dynamic magnetotail behaviour such as during current sheet flapping,
33 particularly at locations where magnetotail flaring becomes dominant.

34

35 **1. Introduction**

36

37 Convective magnetotail plasma flows at Earth, driven by the closing of magnetic flux via
38 reconnection as part of the Dungey Cycle (Dungey, 1961) have been studied extensively for
39 many years (e.g. Angelopoulos et al. 1992, 1994; Sergeev et al., 1996; Petrukovich et al.,
40 2001; Cao et al., 2006; McPherron et al., 2011; Frühauff & Glassmeier, 2016). Arguably, the
41 most well studied of these is the Bursty Bulk Flow (BBF). Angelopoulos et al. (1994) defined
42 BBFs as being channels of earthward plasma flow continually above 100 km s^{-1} , exceeding
43 400 km s^{-1} at one point across some interval, usually across a timescale of a few minutes.
44 The flows are said to be the main transporter of mass, energy and flux in the magnetotail
45 (e.g. Angelopoulos et al., 1994; Nakamura et al., 2002; Grocott et al., 2004c; Kiehas et al.,
46 2018). Although their earthward nature is the key defining characteristic of BBFs, they will
47 invariably exhibit a dusk-dawn component in their bulk flow as well (e.g. Angelopoulos et
48 al., 1994; Petrukovich et al., 2001; Grocott et al., 2004b). Understanding the drivers of dusk-
49 dawn asymmetries in magnetospheric dynamics is an important element of geospace
50 research (e.g. Haaland et al., 2017).

51

52 Magnetotail flows are generally expected to be symmetric about midnight (e.g. Kissinger et
53 al., 2012). A key factor that has been observed to influence the dusk-dawn direction of the
54 magnetotail flow, however, is the B_y component of the Interplanetary Magnetic Field (IMF).
55 It is well established that when the IMF reconnects with the dayside terrestrial magnetic
56 field, a non-zero IMF B_y component leads to asymmetric loading of open flux into the polar
57 cap (e.g. Khurana et al., 1996; Tenfjord et al., 2015; Grocott et al., 2017; Ohma et al., 2019).
58 This results in a twisting of the magnetotail whereby the closed field lines are rotated about
59 the midnight meridian, and a B_y component is superimposed onto the tail field as a
60 consequence of IMF B_y penetration (Cowley, 1981; Petrukovich, 2011; Tenfjord et al., 2015).
61 Subsequently, following nightside reconnection, the tail will untwist (Grocott et al., 2004a),
62 with the excitation of multiple convective flow bursts, each with an earthward and dusk-
63 dawn component, in the tail and nightside ionosphere (Grocott et al., 2007). In order to be

64 consistent with the tail ‘untwisting hypothesis’, any convective flows associated with an
65 individual tail field line should share the same dusk-dawn direction (e.g. see Figure 3 of
66 Grocott et al., 2005). The role of IMF B_y in the untwisting hypothesis has been examined
67 previously in a number of studies (e.g. Grocott et al, 2007; Pitkänen et al., 2013, 2015,
68 2017). These studies revealed that under prolonged positive IMF B_y conditions, the
69 earthward flows are expected to exhibit a dawnward component in the northern
70 hemisphere ($B_x > 0$) and a duskward component in the southern hemisphere ($B_x < 0$), with
71 the opposite correlation for negative IMF B_y conditions. This is especially true close to
72 midnight, where the penetration of IMF B_y is particularly noticeable. Further away from
73 midnight, however, effects such as magnetotail flaring (Fairfield, 1979) are expected to
74 product a dominant B_y component, which may suppress IMF B_y -effects on the dusk-dawn
75 asymmetry, resulting in the symmetric earthward convection of field lines (e.g. see Fig. 2 of
76 Pitkänen et al., 2019). Nevertheless, IMF B_y has been shown to govern the dusk-dawn
77 nature of these flows both during periods of steadier, slower convection (Pitkänen et al.,
78 2019), as well as during more transient, dynamic BBF-like intervals (Grocott et al., 2007) at
79 $|Y_{GSM}|$ values up to 7 R_E (Pitkänen et al., 2013). In the present study, we present Cluster
80 observations of dawnward and duskward directed flows that do not match this expected
81 dependence on IMF B_y , implying that the untwisting hypothesis is insufficient in this case. In
82 particular, we highlight the problematic nature of the observation of dawnward flow, in
83 relation to the pre-midnight location of Cluster. We instead suggest that the flows are being
84 driven by local perturbations due to dynamic behaviour of the tail that are associated with
85 flapping of the current sheet.

86

87 The current sheet, or ‘neutral’ sheet, lies in the equatorial plane at the center of the tail
88 plasma sheet and separates the earthward ($B_x > 0$) and tailward ($B_x < 0$) directed field (Ness,
89 1965). The current sheet is a highly dynamic region of the Earth’s magnetotail which can
90 undergo various types of net motion, such as tilting due to lobe magnetic pressures (Cowley
91 et al., 1981; Tenfjord et al., 2017) as well as flapping. Flapping of the current sheet can
92 generally be described as a sinusoidal-like variation in B_x of up to tens of nanoTesla, where
93 an observing spacecraft often measures repeated changes in the sign of B_x (e.g. Runov et al.,
94 2009), indicative of crossings of the current sheet, with characteristic times ranging from a
95 few seconds to (more commonly) several minutes (e.g. Runov et al., 2009; Wu et al., 2016;

96 Wei et al., 2019). Drivers of current sheet flapping have been widely investigated, with
97 possible causes ranging from external solar wind/IMF changes (Runov et al., 2009),
98 induction of hemispheric plasma asymmetries (Malova et al., 2007; Wei et al., 2015), fast
99 earthward flow (Nakamura et al., 2009) as well as periodical, unsteady magnetotail
100 reconnection (Wei et al., 2019). Studies such as Volwerk et al. (2008) and Kubyshkina et al.
101 (2014) have illustrated that flapping of the current sheet can be associated with variable
102 dusk-dawn flow, potentially overriding, or preventing any IMF B_y control of the flow.

103

104 In this paper we present Cluster spacecraft observations of an interval of dynamic
105 magnetotail behaviour on 12 October 2006, prior to which the B_y component of the
106 concurrent upstream IMF had been largely positive for several hours. Throughout this
107 interval, Cluster 1 observed oscillations in the magnetic field B_x component, which we
108 attribute to current sheet flapping, concurrent with a series of convective fast flows with
109 significant and variable dusk-dawn components. Observations from Cluster 2, 3 and 4
110 indicated that the spacecraft were at a pre-midnight location where magnetotail flaring was
111 dominating over IMF B_y control of the flows, resulting in the expectation of (symmetrical)
112 duskward return flows (Pitkänen et al., 2019). In the southern hemisphere, such duskward
113 flow was measured by Cluster 3, but not observed by Cluster 1, which instead measured
114 flows with significant dawnward components. These dawnward flows were therefore
115 inconsistent with any expectation that the flow was governed by flaring and, owing to
116 evidence of large-scale IMF $B_y > 0$ ionospheric convection pattern, could also not be
117 explained by the magnetotail untwisting hypothesis. We instead suggest that the current
118 sheet flapping was exciting the variable dusk-dawn flow, overriding the expected large-scale
119 duskward convection at the location of Cluster 1.

120

121 **2. Instrumentation and Data Sets**

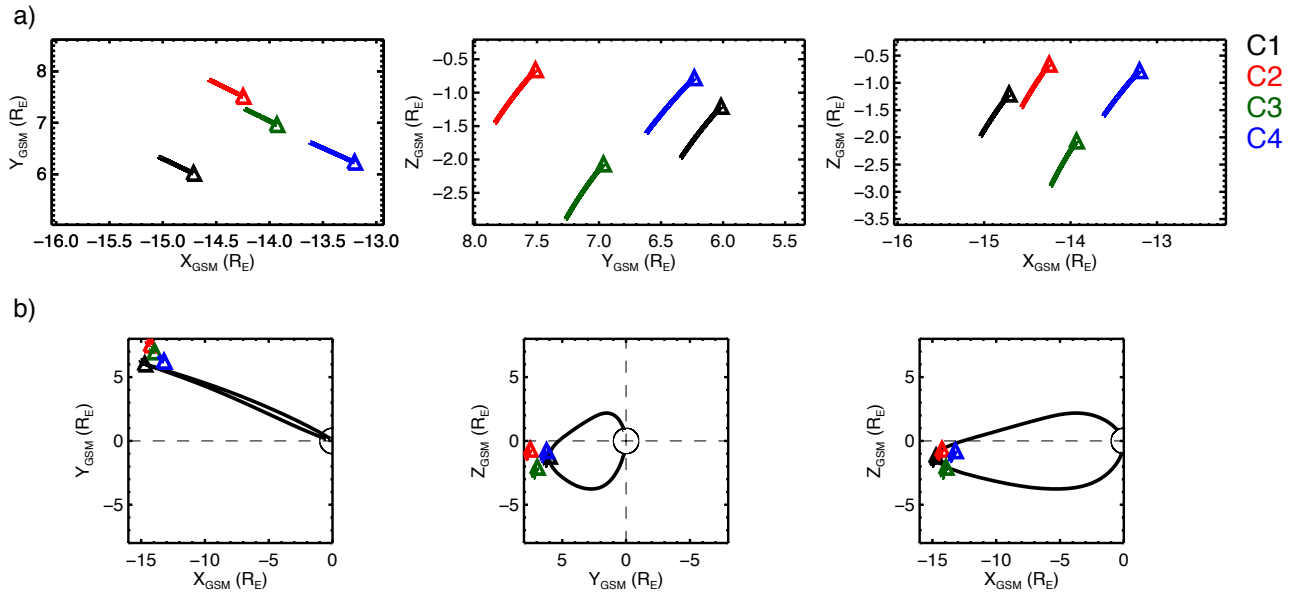
122 *2.1. Spacecraft Data*

123 The magnetospheric observations presented in this case study were made by the Cluster
124 multi-spacecraft (C1-C4) constellation (Escoubet et al., 2001). We make use of the fluxgate
125 magnetometer (FGM) onboard the Cluster spacecraft to obtain magnetic field
126 measurements (Balogh et al., 2001), and obtain our bulk ion velocity data from the Hot Ion
127 Analyser (HIA) on C1 and C3 calculated as on-board moments (Rème et al., 1997). The

128 magnetic field data presented are 5 vectors-per-second (0.2s res) which have been 1s
129 median-averaged, with the velocity data presented having spin resolution of just over 4s.
130 Where these datasets have been combined to produce parameters such as the plasma beta
131 and field-perpendicular velocities, we have resampled both the magnetic field and plasma
132 data to 5s resolution. All data are presented in geocentric solar magnetospheric (GSM)
133 coordinates unless stated otherwise.

134

135 The interval of study in this paper occurred between 00:00 – 00:55 UT on 12 October 2006.
136 At 00:00 UT the Cluster spacecraft were located in the near-Earth magnetotail plasma sheet,
137 in the pre-midnight sector. C1 was located at ($X = -14.7$, $Y = 6.0$, $Z = -1.2$) R_E , C2 at ($X =$
138 -14.2 , $Y = 7.5$, $Z = -0.7$) R_E , C3 at ($X = -13.9$, $Y = 7.0$, $Z = -2.1$) R_E , and C4 at ($X = -13.2$, $Y = 6.2$,
139 $Z = -0.8$) R_E . This is depicted in Fig. 1a by the coloured triangles, along with the respective
140 spacecraft trajectories, from 00:00 – 00:55 UT, by the solid lines. Fig. 1b shows a zoomed-
141 out version of Fig. 1a, which illustrates the location of the spacecraft with respect to the
142 Earth. Fig. 1b also shows a traced modelled magnetic field line, achieved using the semi-
143 empirical TA15 model of the magnetosphere (Tsyganenko & Andreeva, 2015), which passes
144 through the location of C1 and connects to both the northern and southern hemispheres of
145 the Earth. We parameterised the TA15 model using mean-averaged solar wind dynamic
146 pressure (P_{dyn}), IMF B_y and IMF B_z data from the 1-hour interval prior to 00:28 UT (the start
147 of our specific interval of interest). These values were $P_{dyn} = 1.56$ nPa, IMF $B_y = +1.56$ nT and
148 IMF $B_z = -2.17$ nT. There was also a tailward dipole tilt of $\approx -12^\circ$. The model was also
149 parameterised with a solar wind coupling function index known as the ‘N index’, after
150 Newell et al. (2007). The N index varies between 0 (quiet) and 2 (very active), and in this
151 instance was ~ 0.4 .



152

153 **Figure 1:** a) The locations of the Cluster spacecraft in the X-Y, Y-Z, and X-Z GSM planes, from
 154 left to right, respectively, at 00:00 UT on 12 October 2006, marked by the triangles. The
 155 trajectories from 00:00 UT to 00:55 UT are marked by the solid lines. The spacecraft are
 156 colour-coded according to the key on the right. b) As in a), with a zoomed-out view. The
 157 Earth is shown by the solid circle. A TA15 model magnetic field line passing through the
 158 location of C1 is shown as the solid black line.

159

160 The IMF measurements used in this study were provided by the OMNIweb database at 1-
 161 minute resolution, having been first propagated from L1 to the bow shock nose (King &
 162 Papitashvili, 2005).

163

164 2.2. SuperDARN Data

165 The ionospheric observations presented in Sect. 3.3 were provided by the Super Dual
 166 Auroral Radar Network (SuperDARN), an international collaboration of 36 ground-based
 167 radars (Nishitani et al., 2019) that make line-of-sight Doppler measurements of the
 168 horizontal motion of the ionospheric plasma every few seconds (e.g. Chisham et al., 2007).
 169 Here, we use 2-min ionospheric convection maps created by fitting the line-of-sight $\mathbf{E} \times \mathbf{B}$
 170 velocity data to an eighth order expansion of the ionospheric electric potential in spherical
 171 harmonics using the technique of Ruohoniemi & Baker (1998), implemented in the Radar
 172 Software Toolkit (RST version 4.2, 2018). To accommodate intervals with limited data
 173 availability, the data are supplemented with values derived from a statistical model

174 parameterised by IMF conditions. This is a well-established technique that has been
175 thoroughly discussed by, e.g., Chisham et al. (2007). The convection maps we present
176 employ the commonly used model of Ruohoniemi & Greenwald (1996). As a check on the
177 sensitivity of the maps to the choice of model input, we also tested the fitting using the
178 alternative model of Thomas and Shepherd (2018) and found that this has little impact on
179 the maps and no impact on our conclusions.

180

181 As a further measure to ensure that the choice of model is not critical to our results, we
182 chose not to use the concurrent IMF vector to parameterise the background model. In this
183 case, because we are using the SuperDARN data to provide evidence in support of the
184 expected large-scale influence of IMF B_y , we deemed it inappropriate to include model data
185 already parametrised by IMF B_y . We instead specify a nominal southward IMF with zero B_y
186 component in our analysis, to ensure that a background model with no pre-existing IMF B_y
187 influence is used. Although this might result in the patterns we show being less accurate
188 overall, especially in regions of poor data coverage, it will ensure that any B_y -associated
189 asymmetry in the maps is driven by the radar data from our interval of study, and not the
190 background model. This is discussed further in Sect. 4.1, below.

191

192 **3 Observations**

193

194 In this section we present observations of the IMF, magnetotail magnetic field and plasma
195 flow, and ionospheric convection from an interval on 12 October 2006.

196

197 *3.1 IMF Observations*

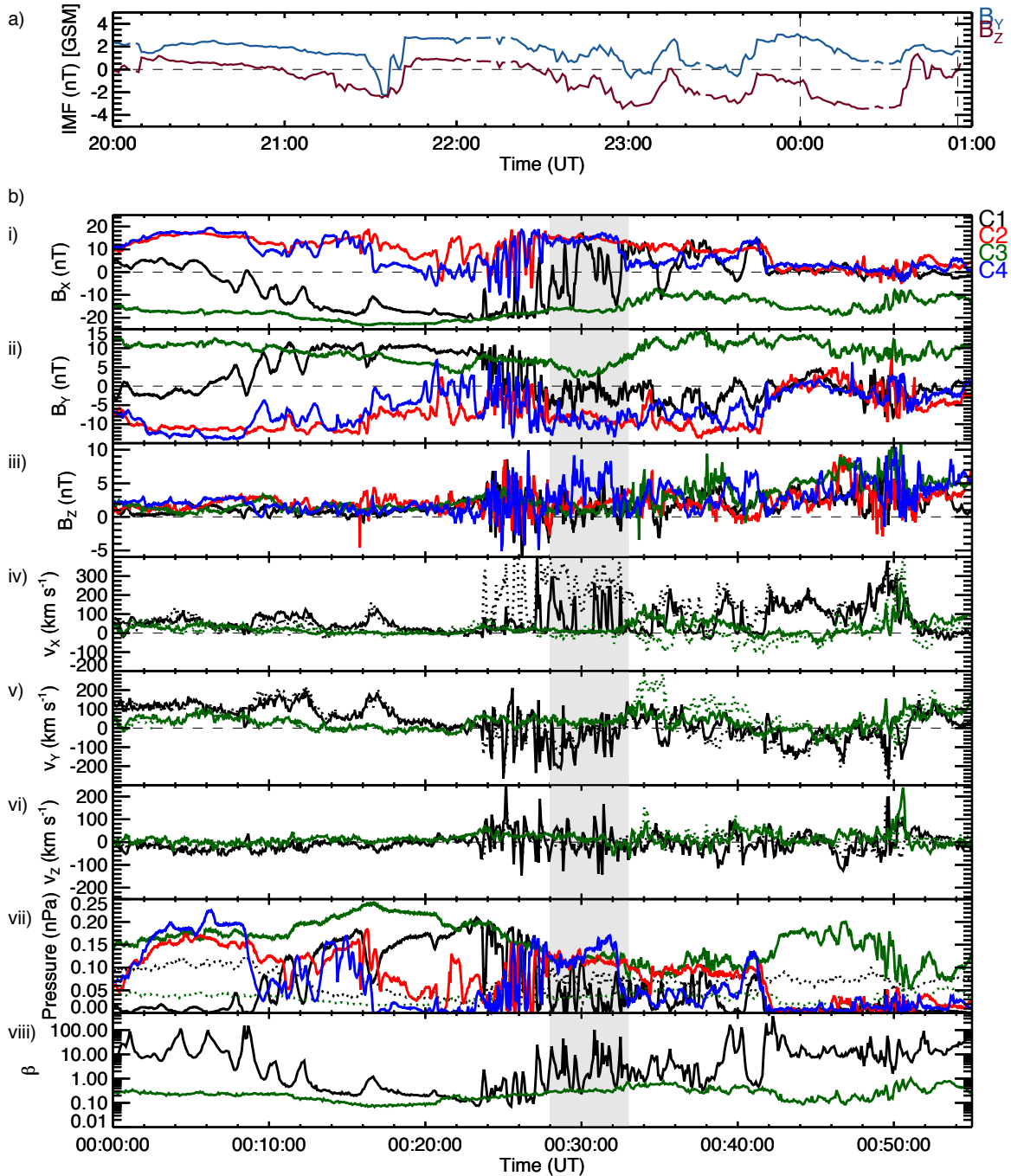
198 Figure 2 presents an overview of the spacecraft data from an extended interval around our
199 period of specific interest for broader context. In Figure 2a, we show a time-series of the
200 IMF B_y and IMF B_z data from 20:00 UT on 11 October to 01:00 UT on 12 October 2006. These
201 data reveal that IMF B_y was generally positive for several hours prior to the fast flow
202 interval, with IMF B_z predominantly negative. There were three small intervals of negative
203 IMF B_y at \sim 21:35 UT, 23:00 UT and 23:40 UT and we discuss the possible ramifications of
204 these, and our treatment of them, in Sect. 4.1.

205

206 3.2 Cluster Spacecraft Observations

207 In Figure 2b, we present the in-situ magnetic field and plasma measurements from the
 208 Cluster spacecraft across the interval 00:00 – 00:55 UT.

209



210

211 **Figure 2:** a) A plot of the IMF time series data for the IMF B_y (blue) and IMF B_z (red)
 212 components, from 20:00 UT on 11 October 2006 to 01:00 UT on 12 October 2006. The
 213 vertical dashed lines indicate the start (00:00 UT) and end (00:55 UT) of the interval of

214 Cluster data (below). b) The in-situ Cluster spacecraft measurements. Shown first is the local
 215 magnetic field data, i) B_x , ii) B_y and iii) B_z , followed by the bulk ion velocity data, iv) v_x , v) v_y ,
 216 and vi) v_z (dotted lines). The field-perpendicular component of the ion flow (indicative of
 217 the $\mathbf{E} \times \mathbf{B}$ convection) is shown in panels iv) to vi) by the solid lines. In panel vii) the magnetic
 218 $\left(\frac{B^2}{2\mu_0}\right)$ and thermal ion (nkT) pressures are shown by the solid and dotted lines respectively,
 219 and in panel viii) the ion plasma beta from C1 and C3 is shown. All data are labelled
 220 according to the colour-coded key on the right-hand side. The time-interval between the
 221 gray shaded region marks our specific interval of interest (discussed in text).

222

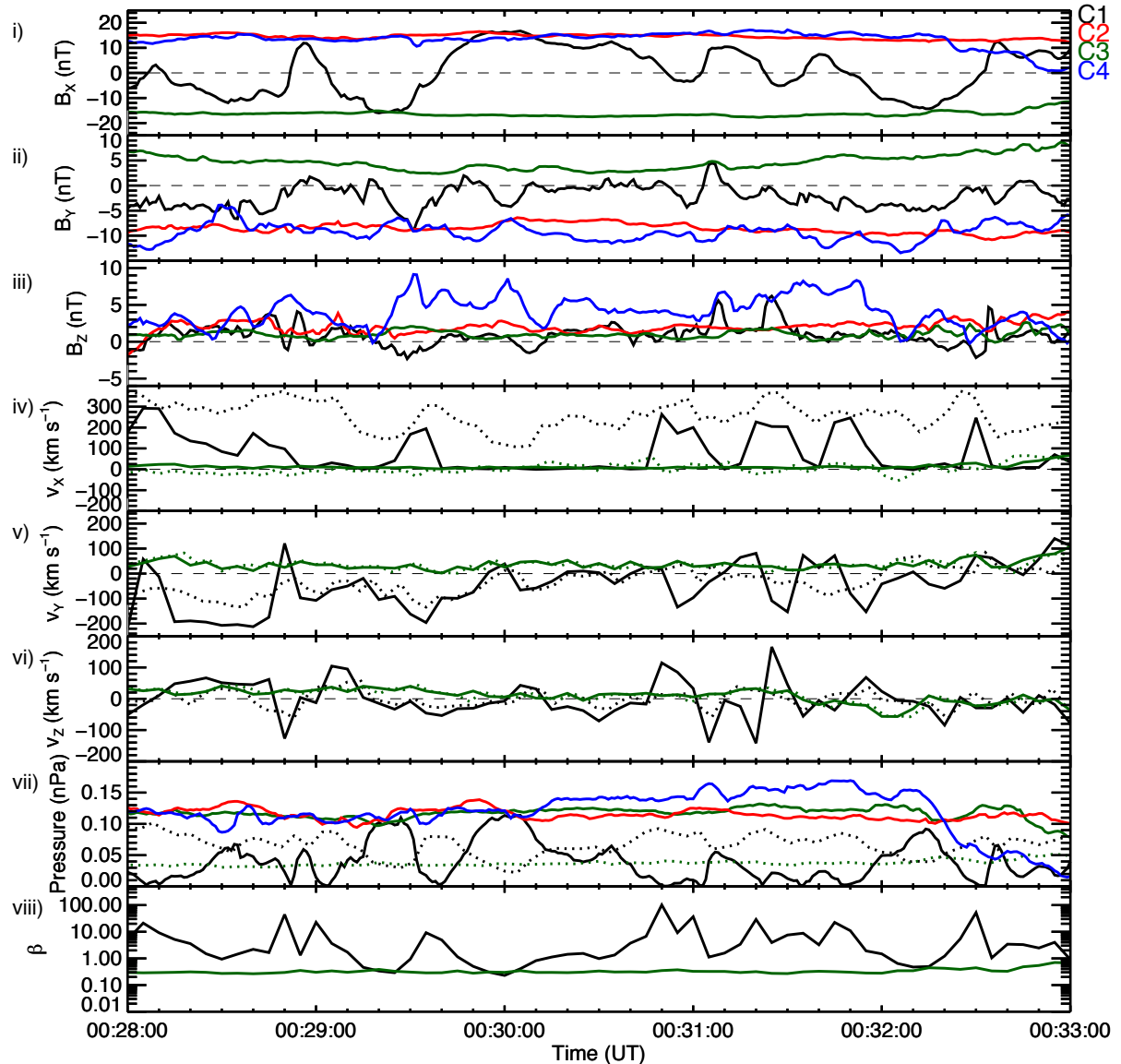
223

224 At $\sim 00:06$ UT, C1 crossed from the northern hemisphere into the southern hemisphere,
 225 illustrated by the sign change in B_x from positive to negative shown in Fig. 2b i). Coincident
 226 with this, the observed B_y , shown in Fig. 2b ii) turned from negative to positive, consistent
 227 with the expected B_y due to magnetotail flaring (see Sect. 4.2) at this pre-midnight location
 228 (Fairfield, 1979). Fig. 2b iv) reveals that up until $\sim 00:24$ UT, the bulk earthward flow (v_x ,
 229 dotted lines) and field-perpendicular flow ($v_{\perp x}$, solid lines) measured by both C1 and C3 was
 230 generally low in magnitude ($< 100 \text{ km s}^{-1}$). The dusk-dawn (v_y) component of the flow,
 231 shown in Fig. 2b v), remained steadily duskward ($v_y > 0$) at C1 and duskward or close to zero
 232 at C3. The north-south (v_z) component of the flow in Fig. 2b vi), measured by C1 and C3 was
 233 effectively zero. During this period, the Cluster spacecraft that resided in the northern
 234 hemisphere (predominantly C2 and C4), observed $B_y < 0$, and the spacecraft which resided
 235 in the southern hemisphere (predominantly C1 and C3) observed $B_y > 0$, again consistent
 236 with magnetotail flaring. Occasionally a spacecraft encountered the current sheet ($B_x = 0$) at
 237 which point it observed $B_y = 0$. We comment on the significance of these magnetic field
 238 observations in Sect. 4.2.

239

240 After $\sim 00:24$ UT, C1 began to observe a period of enhanced earthward flow
 241 ($v_x > 300 \text{ km s}^{-1}$) and variable dusk-dawn flow, concurrent with sudden variation in the local
 242 B_x component. Similarly, C2 and C4, but not C3, observed large magnitude ($> 20 \text{ nT}$) rapid
 243 variations in B_x , which appear to have an apparent timescale of around a minute and which
 244 we attribute to a flapping of the current sheet. As well as rapid variations in B_x , both the B_y

245 and B_z components of C1, C2 and C4 seemed highly variable. As perhaps to be expected,
246 these variations in the magnetic field were accompanied by significant variations in the
247 magnetic pressure of ~ 0.15 nPa, as shown by the solid lines in Fig. 2b vii).
248 Unlike the other spacecraft, C3 remained in the southern hemisphere throughout the entire
249 interval and did not observe the rapid fluctuations in B_x . Between 00:28 – 00:33 UT (the gray
250 shaded region), C1 began to repeatedly and rapidly cross the current sheet, as previously
251 experienced by C2 and C4, whilst continually observing enhanced earthward flow and
252 variable dusk-dawn convective flow ($v_{\perp y}$). Across the entire interval, the plasma beta, β ,
253 indicated in Fig. 2b viii), measured by C3 remained above ~ 0.1 , with C1's measured β
254 ranging from 0.1 to over 100. This is consistent with the fact that C1 was continually
255 crossing the current sheet at the center of the plasma sheet, where β is larger (Baumjohann
256 et al., 1989). It is this interval of current sheet crossing and variable flow observed by C1
257 that we focus on below and is presented in more detail in Figure 3.



258
 259 **Figure 3:** As in Fig. 2b, but for the interval 00:28 – 00:33 UT on 12 October 2006.

260
 261 Fig. 3 i) conveys the extent of the large-amplitude B_x variations observed by C1 between
 262 00:28 and 00:33 UT. B_x was generally fluctuating between positive and negative values
 263 throughout the five-minute interval, with a minimum at ~ -16 nT and maximum at ~ 17 nT.
 264 The magnetic pressure at C1 shown by the solid black line in Fig. 3 vii) is consistent with the
 265 idea that C1 was crossing the current sheet, as this generally reached minima at the center
 266 of each current sheet crossing ($B_x \approx 0$). The B_y component (Fig. 3ii) measured by C1 generally
 267 remained negative and highly variable for the entire interval, with a number of large
 268 negative enhancements and a few small positive excursions. It is particularly of note that
 269 when C1 was below the neutral sheet, as implied by a negative B_x component, B_y was

270 almost always negative. As we discuss in Sect. 4.2, this is inconsistent with what we would
 271 expect based on the location of the spacecraft and also inconsistent with any expectation
 272 that a positive IMF B_y should have penetrated into the tail. The B_z component (Fig. 3iii)
 273 generally remained positive with some small negative excursions.

274

275 Unlike C1, C2-4 measured generally steady B_x throughout this five-minute period. C2 and C4
 276 measured positive B_x , indicating that they were above the neutral sheet, and C3 measured
 277 negative B_x , indicating that it was below the neutral sheet. Similarly, B_y was steadily negative
 278 for C2 and C4 and steadily positive for C3. These observations are consistent with the larger-
 279 scale B_y at the spacecraft location being dominated by magnetotail flaring. Again, we note
 280 the inconsistency between the C1 and C3 observations of B_y ; when in the southern
 281 hemisphere C1 generally observed $B_y < 0$, whereas C3 observed $B_y > 0$. On a few separate
 282 occasions C1 did briefly observe $B_y > 0$ (e.g. at 00:31:05 UT) but at these times C1 was
 283 located above the neutral sheet ($B_x > 0$), while C2 and C4 observed $B_y < 0$ above the neutral
 284 sheet. These variations in B_y imply the observation of a ‘kink’ in the field at the location of
 285 C1, the ramifications of which are discussed further in Sect. 4.2.

286

287 At times when B_x observed by C1 was negative, indicating that C1 was below the neutral
 288 sheet, C1 generally observed negative (dawnward) $v_{\perp y}$ (Fig. 3v) with a magnitude varying
 289 between 100 and 200 km s⁻¹. At times when B_x became positive, indicating that C1 was
 290 above the neutral sheet, C1 observed positive (duskward) $v_{\perp y}$ a majority of the time,
 291 although this flow barely reached 100 km s⁻¹. The negative enhancements in $v_{\perp y}$ were
 292 generally accompanied by negative enhancements in B_y . Across the interval, there was a
 293 near continual $v_x > 200$ km s⁻¹ flow (black dotted line in Fig. 3iv), peaking at almost 400 km
 294 s⁻¹, with concurrent peaks in the convective $v_{\perp x}$ component (solid black line) of at least
 295 200 km s⁻¹. The convective flow measured by C3, however, was generally very weak ($|v_{\perp}| <$
 296 50 km s⁻¹) throughout this period (solid green line in Fig 3iv). v_z (Fig. 3vi), as measured by
 297 both C1 and C3 remained low in magnitude (< 100 km s⁻¹) for the duration of the interval,
 298 with a few $v_{\perp z}$ excursions above 100 km s⁻¹ observed by C1. The most significant
 299 enhancements in $v_{\perp z}$ seen by C1 appeared to occur in conjunction with the rapid current
 300 sheet crossings between 00:30:50 and 00:32:00 UT. We discuss the implications of these

301 observations in the context of the upstream IMF conditions and large-scale magnetospheric
302 morphology in Sect. 4.

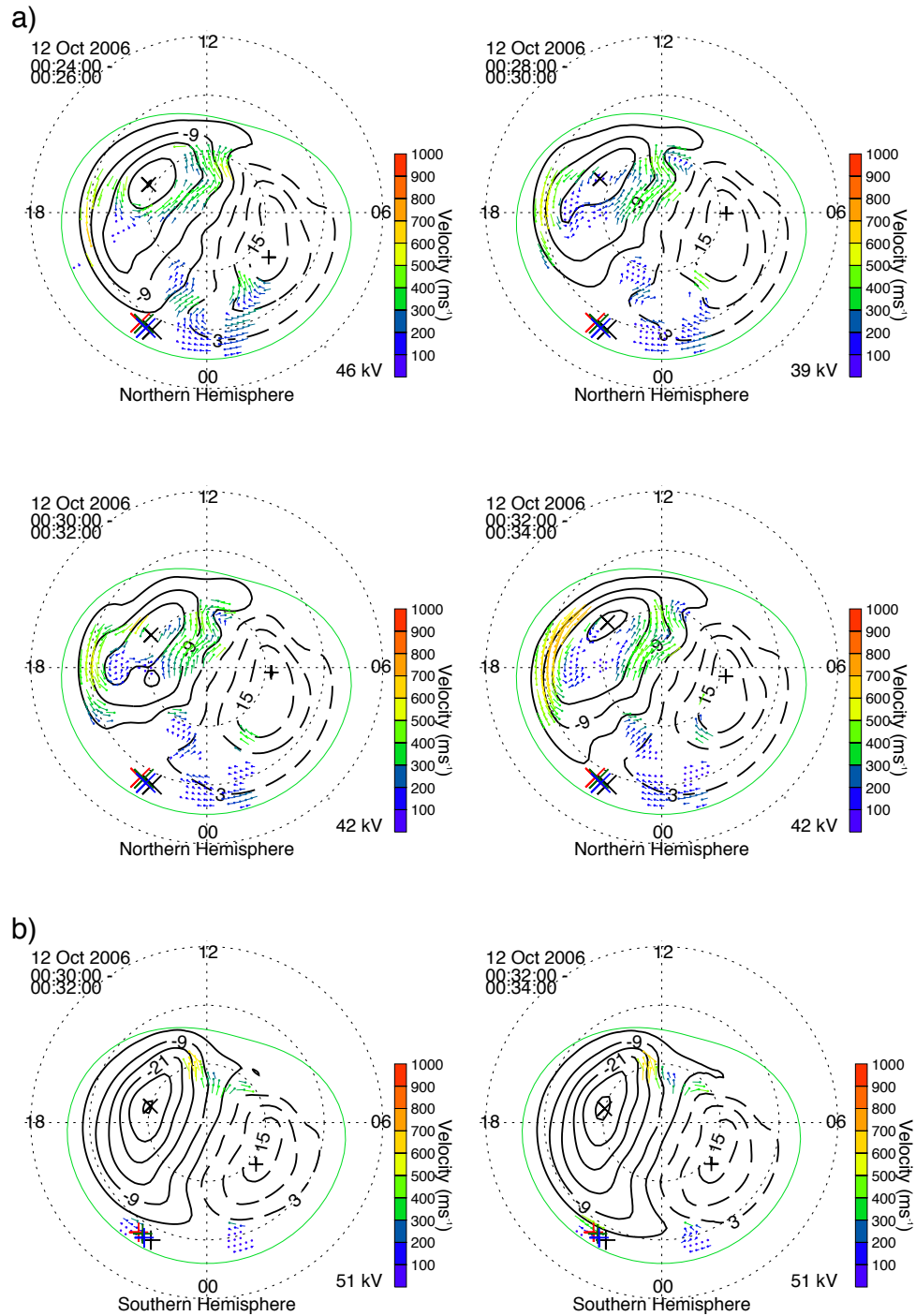
303

304

305 *3.3 Ionospheric Convection Observations*

306

307 To provide the large-scale context in which we can interpret the more localised
308 observations from the Cluster spacecraft we show ionospheric convection observations in
309 Figure 4. In Fig. 4a we present a series of four 2-minute integration SuperDARN maps of the
310 northern hemisphere ionospheric convection pattern, beginning at 00:24 UT, and ending at
311 00:34 UT, which encompasses our specific interval. In all maps, plasma is flowing anti-
312 sunward across the polar cap at high latitudes, also with a strong duskward sense, with the
313 direction of the convection reversing in the pre-midnight sector before returning sunward at
314 lower latitudes.



315

316

317

318

319

320

321

322

Figure 4: Maps of the ionospheric plasma convection derived from SuperDARN observations. Midnight is to the bottom of each map, noon to the top, dusk to the left and dawn to the right. The dashed black circles are spaced every 10° in magnetic latitude. The thicker solid and dashed black lines represent the plasma streamlines and are the contours of the electrostatic potential. Flow vectors are plotted at the locations of radar observations and these are colour-coded based on the magnitude of their velocity. a) Four 2-minute northern hemisphere maps from 00:24 – 00:26, 00:28 – 00:30, 00:30 – 00:32 and 00:32 –

323 00:34 UT, respectively. b) Two 2-minute southern hemisphere maps from 00:30 – 00:32 and
324 00:32 – 00:34 UT, respectively. On each northern (southern) hemisphere map, the
325 footpoints of the Cluster spacecraft constellation are shown by the X's (+'s), mapped using
326 the TA15 model.

327

328

329 Owing to the coupled nature of the magnetosphere-ionosphere system, the observed
330 ionospheric convection pattern is indicative of the global-scale magnetospheric convection
331 (Cowley, 1981). In this case, the typical symmetrical twin-cell convection pattern has been
332 rotated clockwise, with the dawn cell extending across into the pre-midnight sector,
333 indicative of convection that has been driven under the influence of a positive IMF B_y
334 component (e.g. Reistad et al., 2016, 2018). On each northern hemisphere map, the
335 footpoints of the Cluster spacecraft constellation are indicated by the crosses (X), mapped
336 using the TA15 model with the same parameterisation described in Sect. 2.

337

338 Fig. 4b shows two 2-minute integration SuperDARN maps of the southern hemisphere
339 ionospheric convection pattern, beginning at 00:30 UT, and ending at 00:34 UT. The
340 associated footpoints of the Cluster spacecraft are indicated by the plus signs (+). Although
341 the coverage of radar data is much less than in the northern hemisphere, there are data in
342 the pre- and post-midnight sectors which appears to be influencing the location of the flow
343 reversal region at the nightside end of the dusk cell. Opposite to the northern hemisphere
344 case, it is the dusk cell in the south which is extending towards, or just beyond, the midnight
345 meridian. This is also consistent with a large-scale positive IMF B_y influence, owing to the
346 expected north-south asymmetry of the influence of IMF B_y in the magnetosphere (e.g.
347 Pettigrew et al., 2010). The significance of these observations is further discussed in Sect.
348 4.1.

349

350 **4. Analysis and Discussion**

351

352 We have presented observations of a dynamic interval of plasma flows and magnetic field in
353 the Earth's magnetotail. In this section we discuss our rationale for interpreting the flows
354 observed by C1 as being inconsistent with the large-scale convection expected based on the

355 spacecraft location and magnetotail untwisting considerations, and our alternative
356 interpretation of their relationship to current sheet flapping.

357

358 *4.1 Evidence for an inconsistency with large-scale magnetotail untwisting*

359 During the five-minute interval studied (00:28 – 00:33 UT) C1 measured a continually
360 fluctuating B_x component (Fig. 3i), indicative of multiple crossings of the tail current sheet.
361 C1 was the only spacecraft to measure this signature across the interval (although similar
362 signatures had been observed a few minutes earlier by C2 and C4). C1 also measured a
363 series of earthward convective magnetotail fast flows with varying dusk-dawn components.
364 The data in Fig. 3 i) and Fig. 3 v) illustrate that when B_x was positive (negative), a duskward
365 (dawnward) $v_{\perp y}$ was generally observed. The observed dawnward flow in the southern
366 hemisphere, in particular, is inconsistent with the expected symmetric duskward flow at the
367 pre-midnight location of C1 which was, however, observed by C3. This suggests that the
368 typical ‘symmetrical’ Dungey-cycle return flow (e.g. Kissinger et al., 2012) cannot provide an
369 explanation for the flow observations made by C1. We thus turn our attention to other
370 possible explanations which we explore in detail, below.

371

372 The data in Fig. 3 ii) show that C1 tended to observe a negative B_y component. According to
373 the magnetotail untwisting hypothesis (e.g. Pitkänen et al., 2015), these flow and magnetic
374 field observations are consistent with a negative IMF B_y penetration. The IMF data
375 presented in Fig. 2a, on the other hand, revealed that IMF B_y was generally positive for
376 several hours prior to the fast flow interval (00:28 – 00:33 UT). Based on the IMF data alone,
377 therefore, one might expect that a positive IMF B_y will have penetrated into the
378 magnetosphere and thus ought to have determined the “expected” dusk-dawn direction of
379 the flow. In that case, the flows observed here would have a dusk-dawn sense that is not
380 explained by current theoretical models of magnetotail untwisting, meaning they are not
381 IMF B_y -controlled (e.g. Grocott et al., 2007). There are a number of possible explanations for
382 this discrepancy and we address each one in turn.

383

384 The first possibility is that our conclusion regarding the expected sense of IMF B_y control is
385 incorrect. As discussed above, the flows observed by Cluster would be consistent with the
386 magnetotail untwisting hypothesis in the case that we had IMF $B_y < 0$ penetration. We

387 noted in Sect. 3.1 that there were three small negative IMF B_y excursions prior to our Cluster
388 observations interval. Although the propagation of the IMF to the bow shock is accounted
389 for in the OMNI data, there is uncertainty regarding the time it takes for the IMF B_y to
390 'propagate' into the magnetotail. Uncertainties in IMF B_y propagation times (e.g. Case &
391 Wild, 2012) have previously been cited as an explanation for observing an unexpected
392 asymmetry (e.g. Pitkänen et al., 2013). Studies such as Tenfjord et al. (2015, 2017) and Case
393 et al. (2018), for example, have suggested a reconfiguration time (to the prevailing IMF B_y
394 conditions) for nightside closed field lines of around 40 minutes. At ~00:28 UT (the
395 beginning of our specific interval of interest), the IMF B_y had been positive for around
396 50 minutes. Based on the Tenfjord timescale, this would thus imply that our interval was
397 wholly IMF $B_y > 0$ driven. Other studies, on the other hand, such as Browett et al. (2017),
398 have shown that longer timescales of a few hours may be important.

399

400 However, for such long timescales to play a role one would expect to have observed a
401 relatively persistent IMF B_y component during that time. The integrated IMF B_y over the
402 hours prior to our interval was certainly convincingly B_y -positive, and it seems highly unlikely
403 that a few minute-long fluctuations into the opposite IMF B_y polarity, 1 or 2 hours prior to
404 the flows we observed, could have a significant influence. We can thus be confident that
405 positive IMF B_y was governing the global magnetospheric dynamics in this case.

406

407 Despite this convincing argument that the IMF data alone imply a positive IMF B_y
408 penetration, we performed an additional analysis to further ensure that these negative
409 excursions did not lead to a change in the global nature of the magnetosphere-ionosphere
410 system. We inspected the concurrent northern hemisphere SuperDARN data (presented in
411 Fig. 4a) to provide evidence of the large-scale convection pattern. If the large-scale flow is
412 consistent with a positive IMF B_y component, then the magnetotail flows that we observed
413 must be deviating from this for some reason and cannot be related to IMF B_y control. The
414 SuperDARN data indeed confirm that the large-scale morphology of the system was
415 consistent with a positive IMF B_y component (e.g. Lockwood 1993; Grocott et al., 2017;
416 Reistad et al., 2018). This can be inferred from the general shape of the convection pattern,
417 whereby across multiple maps (00:24 – 00:34 UT) the pattern was rotated clockwise, with
418 the dawn cell having extended into the pre-midnight sector. That this is the expected

419 convection pattern for an IMF B_y -driven magnetosphere is also supported by the concurrent
420 low level of geomagnetic activity. The auroral AU and AL indices (not shown) confirm that
421 this interval is geomagnetically quiet (AU and |AL| both less than (or of the order of) 10 nT),
422 such that the nightside ionospheric convection asymmetry should be driven by IMF B_y rather
423 than conductivity-driven features such as the Harang reversal which might otherwise
424 complicate the auroral zone flows (e.g. Grocott et al., 2007; Grocott et al., 2008; Reistad et
425 al., 2018).

426

427 The validity of the convection observations is further supported by the coverage of nightside
428 data which were used to constrain the model convection pattern. The data used to create a
429 SuperDARN convection map are supplemented by data from a statistical model (in this case
430 Ruohoniemi & Greenwald, 1996) which is typically parameterised by the instantaneous IMF
431 conditions. In the case that there is a lack of real data coverage, a created SuperDARN map
432 will be strongly influenced by the model data, as opposed to real data, and thus would
433 reflect a prediction of convection based on the IMF conditions. The maps shown in Fig. 4a
434 illustrate that there were dozens of SuperDARN vectors in the midnight sector which were
435 fitted to create the global convection maps. To confirm that these data were sufficient, and
436 that the observed large-scale convection pattern was not being driven by model data, we
437 parameterised the model in our analysis with IMF $B_y = 0$. Despite this, a clear IMF B_y -
438 asymmetry exists, thus demonstrating that the observed large-scale IMF $B_y > 0$ global
439 convection patterns must be data-driven.

440

441 A second possible explanation for the discrepancy between the dusk-dawn direction of the
442 local and global-scale convection concerns the certainty with which we can determine the
443 location of the spacecraft with respect to the large-scale convection pattern. The untwisting
444 hypothesis, as considered by e.g. Pitkänen et al. (2013, 2017), relies on the assumption that
445 the convection cell to which the spacecraft is connected should be a factor of only
446 hemisphere and the sense of IMF B_y . In other words, as discussed above, for IMF $B_y > 0$, the
447 hypothesis dictates that C1 ought to be located on the dawn cell when above the neutral
448 sheet and the dusk cell when below, at least in the case that the spacecraft is close to
449 midnight (Grocott et al., 2007). This might be true statistically, but does not account for the
450 dusk-dawn location of the spacecraft, which in this case was $6 \lesssim Y_{\text{GSM}} \lesssim 7 R_E$. If, as a result,

451 the spacecraft was actually located on the dusk cell when above the neutral sheet, and on
452 the dawn cell when below the neutral sheet, then the sense of the observed plasma sheet
453 flows would actually be consistent with the large-scale convection.

454

455 One way to specify which cell the spacecraft is located within is to map its location into the
456 ionosphere. This has been done using TA15 and is shown by the crosses (X) on the northern
457 hemisphere convection maps and by plus signs (+) on the southern hemisphere convection
458 maps, in Fig. 4a and 4b, respectively. For the northern hemisphere maps, there appears to
459 be insufficient scatter to determine the exact division between the dusk and dawn
460 convection cells, such that it is inconclusive as to which cell the Cluster spacecraft map to
461 when above the neutral sheet. If Cluster in-fact mapped to the dusk convection cell,
462 however, then the duskward flows in the northern hemisphere plasma sheet observed by
463 C1 would actually be consistent with the large-scale convection pattern. Furthermore, given
464 that the C2-C4 magnetic field observations are consistent with the local B_y being dominated
465 by magnetotail flaring (as opposed to IMF B_y) at the pre-midnight location of Cluster, it is
466 likely that we would expect the return sense of the convection to be dominated here by the
467 symmetric (duskward) element both above and below the neutral sheet (see e.g. Pitkänen
468 et al., 2019).

469

470 If we instead consider the southern hemisphere maps in Fig. 4b we can be more certain of
471 which cell the spacecraft map to. Owing to the IMF B_y positive nature of the convection (i.e.
472 the more extended southern hemisphere dusk cell) and the pre-midnight location of the
473 spacecraft, the footpoints are located quite convincingly on the dusk cell. This is despite the
474 dusk-dawn asymmetry being less pronounced than that seen in the northern hemisphere
475 (and the associated poorer coverage of southern hemisphere SuperDARN data). When
476 below the neutral sheet C1 observed downward flows, meaning it would have to have been
477 on the southern hemisphere dawn cell to be consistent with the large-scale convection,
478 which is clearly not the case. Indeed, the observed downward flow in the southern
479 hemisphere at this location could only be interpreted in terms of the untwisting hypothesis
480 for a situation where we had clear IMF $B_y < 0$ penetration (and associated extended dawn
481 cell), which has already been ruled out. C3, meanwhile, continually observed duskward flow,
482 which appears to be consistent with the larger-scale convection. It seems much more likely,

483 therefore, that C1 observed flow that was associated with localised magnetic field dynamics
484 rather than being a signature of the large-scale convection.

485

486

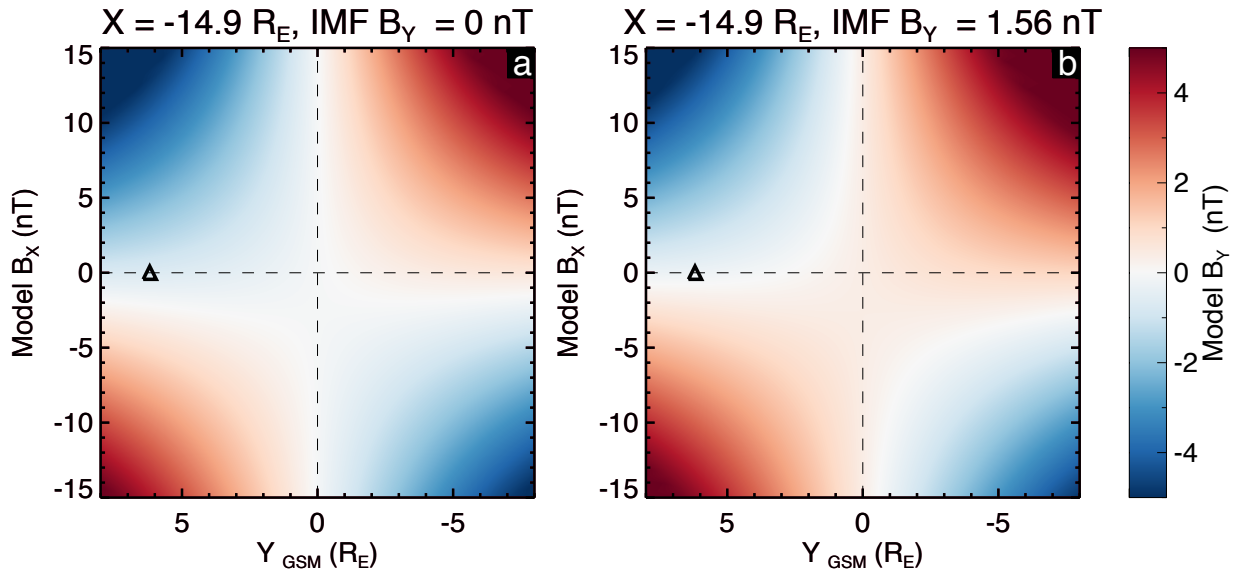
487 *4.2 Evidence for a local perturbation in the magnetotail*

488 The lack of consistency with the large-scale convection leads us to a third explanation for
489 our observations, which is that there is a local perturbation within the tail that is
490 independent of any large-scale, IMF B_y -controlled asymmetry associated with magnetotail
491 untwisting. This is supported by the observations from the other Cluster spacecraft. The
492 low-level of flow seen by C3 is mostly duskward (Fig. 3v), which would be consistent with
493 untwisting for IMF $B_y > 0$, given its southern hemisphere location. We note, however, that
494 due to the pre-midnight location of C3, one would also rightly expect to observe duskward
495 flow even in the case that there was no IMF $B_y > 0$ control (e.g. Kissinger et al., 2012) .
496 Further, in Fig. 2b v), up until the rapid B_x variations began at ~00:24 UT, fast duskward flow
497 in the southern hemisphere was also seen by C1. The fact that C3 continued to then observe
498 steady duskward flow, and no significant B_x change, suggests that the change in the nature
499 of the C1 observations after 00:24 UT must in-fact be due to some localised process that
500 was responsible for driving the dawnward component of the flows which was only observed
501 by C1.

502

503 This idea of a local perturbation is also supported by the variations in the local B_y
504 component. Fig. 3 ii) illustrates the in-situ variations in B_y with time across the interval.
505 Despite there clearly being positive IMF B_y penetration globally (as confirmed by inspection
506 of the OMNI and SuperDARN data), C1, C2 and C4 all recorded mostly negative local B_y
507 values. In the studies of, e.g., Pitkänen et al. (2013, 2017) this observation would have been
508 offered as evidence of a negative of IMF B_y penetration, thus supporting the untwisting
509 hypothesis. However, it is important to note that a negative local B_y component may be
510 wholly consistent with positive IMF B_y . There are, in fact, multiple sources of B_y in the tail,
511 such as magnetotail flaring (Fairfield, 1979), as well as tilt effects and current sheet warping
512 (see e.g. Petrukovich et al., 2005), in addition to a penetration of the IMF B_y . To fully
513 interpret the magnetic field observations, we must therefore consider the possible effects

514 of these phenomena on the presence of B_y in the tail at the specific location of each
 515 spacecraft.



516

517

518 **Figure 5:** TA15 model magnetic field data. In each case, plotted is Y vs B_x [GSM], (at
 519 $X = -14.9 R_E$, i.e. the X position of C1 at $\sim 00:28$ UT on 12 Oct 2006), with the TA15 modelled
 520 B_y value shown by the colour bar on the right. The black triangle shows the Y -location of C1,
 521 at $B_x = 0$. In panel (a) we have imposed IMF $B_y = 0$, and for panel (b) we have used the 1-
 522 hour mean-averaged IMF B_y (+1.56 nT) in the hour prior to 00:28 UT.

523

524 To aid in this interpretation, we present TA15 model magnetic field data in Figure 5, to
 525 provide an indication of the expected background B_y -component at the time of our interval.
 526 These data, from $X = -14.9 R_E$, are plotted against Y [GSM]-position on the horizontal axis,
 527 and against the B_x -component on the vertical axis. We have reversed the conventional
 528 direction of the horizontal axis (negative to positive from left to right) to be consistent with
 529 a view looking earthward from downtail. In panel (a) we show the field for the case that IMF
 530 $B_y = 0$ and in panel (b) the case that IMF $B_y = +1.56$ nT (the 1-hour mean-averaged IMF B_y in
 531 the hour prior to 00:28 UT). The first conclusion we can make from consideration of the B_y
 532 component in Fig. 5a is how, even under no IMF B_y penetration, a ‘background’ B_y value will
 533 exist in the tail purely dependent on location. In such a ‘symmetric’ tail, one would expect
 534 the background B_y value to appear as one moves away from midnight toward the dusk-
 535 dawn flanks, as well as further above and below the neutral sheet. Pre-midnight, we would

536 expect to observe negative B_y above the neutral sheet ($B_x > 0$), and positive B_y below the
 537 neutral sheet ($B_x < 0$), with the opposite effect post-midnight. This is the well-known
 538 magnetotail flaring effect (Fairfield, 1979).

539

540 The data in Fig. 5a also show the effect of the negative (tailward) dipole tilt (as appropriate
 541 to our study interval) and current sheet warping on the local B_y component. According to
 542 Petrukovich (2011), the current sheet warping (controlled by the dipole tilt) is expected to
 543 add a negative B_y component pre-midnight and a positive B_y component post-midnight.
 544 Furthermore, the ‘even tilt’ effect is expected to add a negative B_y component to both the
 545 pre and post-midnight sectors for a negative tilt. This leads to the effect seen in Fig. 5a
 546 where in the pre-midnight sector, the location of the B_y polarity change occurs in the
 547 southern hemisphere (at $B_x \approx -3$ nT).

548

549 Fig. 5b illustrates the scenario relevant to our case study, where we have additionally a
 550 global positive IMF B_y penetration. This additional positive B_y has the effect of moving the
 551 location of the pre-midnight B_y polarity change back up towards the neutral sheet. This
 552 explains why the Cluster spacecraft observed $B_y \approx 0$ at times of $B_x \approx 0$ during the few tens of
 553 minutes prior to our interval, as noted in Sect. 3.2. This also explains why C2-3 and C4
 554 observed the polarity of B_y that they did throughout the interval. It is thus clear that positive
 555 IMF B_y penetration does not mean we should expect to observe positive B_y everywhere in
 556 the tail, rather, it simply means that there is expected to be some positive B_y perturbation
 557 to the already present ‘background’ B_y at a particular location. As Fig. 5b demonstrates, C2
 558 and C4 (located above the neutral sheet) are expected to have observed negative B_y even
 559 though positive IMF B_y has penetrated into the magnetotail, illustrating that the flaring
 560 effect is generally dominant at the spacecraft location. The background B_y expected at their
 561 location (pre-midnight, $B_x > 0$), is negative and the IMF B_y -associated perturbation was not
 562 large enough to enforce a sign change in B_y .

563

564 The Cluster spacecraft in our study were all located pre-midnight (+Y GSM). From Figure 3,
 565 C2 and C4 observed positive B_x , and negative B_y , and at ~00:28 UT were located at around
 566 $Z = -1 R_E$ (Figure 1). C3, however, observed negative B_x and positive B_y , and was located at
 567 around $Z = -2.5 R_E$. The location of the neutral sheet at ~00:28 UT can therefore be said

568 (locally) to have been somewhere between -1 and $-2.5 R_E$ in Z . C1 was located at around $Z =$
 569 $-1.5 R_E$ and, throughout the five-minute interval, observed a B_x which continually fluctuated
 570 from positive to negative, yet observed mostly weakly negative B_y . For B_y to have remained
 571 negative, despite C1 moving above and below the neutral sheet, suggests that there was a
 572 B_y negative 'kink' in the magnetotail that was localised to the vicinity of C1. This is further
 573 supported by the fact that numerous (albeit brief) positive B_y excursions occurred when C1
 574 was above the neutral sheet (as noted in Sect. 3.2). We use the term 'kink' to highlight a
 575 deformation in the nearby field lines which results in the observed perturbations to the local
 576 B_y component. We suggest that this deformation could be relatively small in terms of field
 577 line length, much like a kink in a cable or wire. In the following section, we investigate this
 578 kink in relation to the observed current sheet flapping.

579

580

581 *4.3 Evidence for current sheet flapping as a source of the asymmetric flows*

582 If a localised magnetic field perturbation was associated with the lack of observation of the
 583 expected dusk-dawn flow for magnetotail untwisting, investigating its cause seems a
 584 worthwhile endeavour. The clear sinusoidal-like variation in B_x observed by C1, which is
 585 evidence of current sheet flapping (e.g. Runov et al., 2009), provides us with a starting point
 586 for this investigation. This flapping must be either highly localised or low in amplitude, as at
 587 the time of our five-minute flow interval (00:28 -00:33 UT), only C1 observed the flapping.
 588 MVA analysis (Sonnerup & Cahill, 1967) suggests that the flapping was a kink-like wave
 589 which was propagating downward (Rong et al., 2015; Wu et al., 2016), and therefore may
 590 have been a source of the observed dusk-dawn flow.

591

592 The causes of current sheet flapping have been discussed previously (Runov et al., 2009;
 593 Wei et al., 2019). One such cause has been attributed to localised, periodical reconnection –
 594 a process known to drive Bursty Bulk Flows (BBFs) in the magnetotail (Angelopoulos et al.,
 595 1994; Zhang et al., 2016). In fact, BBFs excited directly as a result of reconnection in the tail
 596 have been previously linked to magnetic fluctuations in the current sheet (Nakamura et al.,
 597 2009; Wu et al., 2016). Examining the data presented in Fig. 3 iii) and Fig. 3 iv), we note that
 598 C1 measured a generally positive B_z , with a few negative blips, as well as continually fast (v_x
 599 $> 200 \text{ km s}^{-1}$) earthward flow, peaking at over 370 km s^{-1} with bursts of enhanced

600 convective flow ($v_{\perp x} > 200 \text{ km s}^{-1}$) also apparent. These observations are fairly consistent
 601 with (if slightly slower than) the original definition of a BBF (Angelopoulos et al., 1994). This,
 602 along with the absence of similar flow observations in the C3 data, suggests that C1 may
 603 have been located earthward of a localised reconnection site (owing to $B_z > 0$), where
 604 persistent, localised reconnection was exciting fast earthward flow. The reconnection
 605 process may then have been driving the current sheet flapping, inducing the localised kink in
 606 the field, and ultimately controlling the dusk-dawn direction of the convective flow.

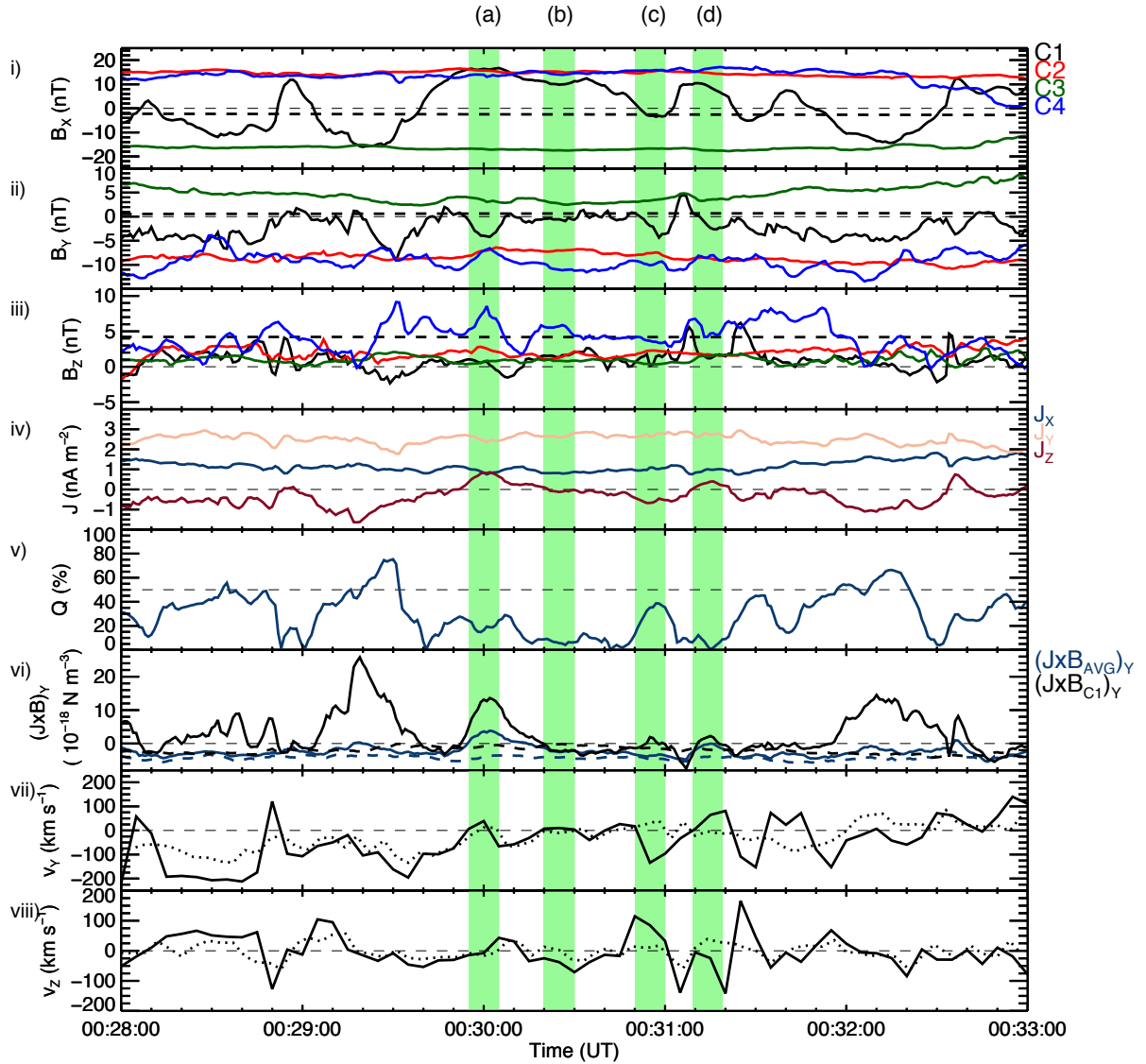
607

608

609 It is well known that the magnetic tension force is responsible for the acceleration of plasma
 610 following reconnection (Karlsson et al., 2015). Our observations of a dusk-dawn flow
 611 component may be related to the localised magnetic tension forces driving and directing
 612 plasma flows in association with the flapping. In order to provide some scope to this
 613 suggestion, we attempted to find the direction of the $\mathbf{J} \times \mathbf{B}$ forces acting on the plasma. We
 614 used the curlometer technique (Dunlop et al., 1988, 2002), to estimate the average current
 615 density, \mathbf{J} , flowing through the volume bound by the spacecraft tetrahedron. The $\mathbf{J} \times \mathbf{B}$
 616 force density [N m^{-3}] is then calculated, firstly, by taking the cross product of \mathbf{J} with the
 617 average magnetic field vector \mathbf{B} from the four-spacecraft (\mathbf{B}_{AVG}). We also calculate $\mathbf{J} \times \mathbf{B}$
 618 using solely \mathbf{B} from C1 (\mathbf{B}_{C1}), in order to provide a more local estimate for $\mathbf{J} \times \mathbf{B}$ at the
 619 location of C1.

620

621 In order to check the validity of using the curlometer approach, we calculated the quality
 622 parameter, Q , defined as $|\nabla \cdot \mathbf{B}|/|\nabla \times \mathbf{B}|$. It is generally accepted that a value of $Q < 0.5$ is
 623 required for a current estimate to be valid. Hence, the value of Q , along with due
 624 consideration of the spacecraft configuration and its orientation relative to the magnetic
 625 field structure, may be used as a monitor of how reliable the curlometer approach is
 626 (Dunlop et al., 2002). This is discussed further below, in reference to the analysis shown in
 627 Figure 6.



628

629 **Figure 6:** i-iii) The local magnetic field vector \mathbf{B} (B_x , B_y , B_z) observed by C1-4, as shown
 630 previously (solid lines) and the TA15 modelled \mathbf{B} vector for C1 (dashed black lines). iv) The
 631 components of the current density vector \mathbf{J} (J_x , J_y , J_z), v) Q , vi) $(\mathbf{J} \times \mathbf{B}_{AVG})_y$ (solid blue line)
 632 and $(\mathbf{J} \times \mathbf{B}_{C1})_y$ (solid black line). The dashed blue and black lines indicate the equivalent
 633 calculation where the TA15 model \mathbf{B} field of C1 has been used (see text). vii) v_y ($v_{\perp y}$ in solid
 634 lines), observed by C1 and viii) v_z ($v_{\perp z}$ in solid lines), also observed by C1. The green
 635 highlighted regions labelled (a), (b), (c) and (d) correspond to four specific time-windows of
 636 interest (discussed in-text).

637

638 Shown in Fig. 6 i-iii) are the local magnetic field B_x , B_y and B_z components, as presented
 639 previously. In Fig. 6 iv) are the current density J_x , J_y and J_z components determined from the

640 curlometer analysis. In Fig. 6 vi) is the dusk-dawn component of $\mathbf{J} \times \mathbf{B}_{AVG}$ and $\mathbf{J} \times \mathbf{B}_{C1}$.
 641 Finally, in Fig. 6 vii) and viii) are the dusk-dawn and north-south components of the flow
 642 (and field-perpendicular flow) observed by C1, as shown previously. In panels (i-iii), the
 643 dashed black line represents the TA15 modelled magnetic field (see Sect. 4.2) at the location
 644 of C1. In panel (vi) the dashed blue and black lines represent the $(\mathbf{J} \times \mathbf{B}_{AVG})_y$ and $(\mathbf{J} \times \mathbf{B}_{C1})_y$
 645 forces, respectively, where \mathbf{J} and $\mathbf{J} \times \mathbf{B}$ have been computed using the model field at the
 646 location of C1 and the true magnetic fields measured by C2-C4. These ‘model $(\mathbf{J} \times \mathbf{B})_y$ forces’
 647 have been computed to provide an illustration of what one would expect the ‘unperturbed’
 648 magnetic field of C1 and the associated $(\mathbf{J} \times \mathbf{B})_y$ force to look like, in the absence of any
 649 dynamical effects such as current sheet flapping or field line ‘kinking’. In both cases, the
 650 model $(\mathbf{J} \times \mathbf{B})_y$ forces are weakly downward, consistent with the ‘background curvature’ of
 651 the magnetic field at this pre-midnight location (see Fig. 7). Fig. 6 v) suggests that our
 652 curlometer approach is generally appropriate, as Q mostly remains below 50% (horizontal
 653 dashed line) for the five-minute interval. We note that, unlike in previous studies which
 654 have used the curlometer technique at inter-spacecraft separation distances of $\ll 1 R_E$ (e.g.
 655 Dunlop et al., 2002; Runov et al., 2003), in our case the Cluster spacecraft separation is large
 656 ($\gtrsim 1 R_E$). Therefore, the curlometer is likely to be an underestimate of the true current at
 657 these scale sizes. Critically, however, the spacecraft configuration is such that the estimate
 658 of the direction of the currents should be stable. Thus, although the volume enclosed by the
 659 spacecraft is greater than the scale sizes of the current sheet flapping and kink, a reliable
 660 estimate of the direction of the net $\mathbf{J} \times \mathbf{B}$ force within the enclosed volume may still be
 661 obtained.

662
 663 Two key features of Figure 6 are apparent. Firstly, it appears as though the perturbations to
 664 $(\mathbf{J} \times \mathbf{B})_y$ are mostly associated with the magnetic field perturbations generally only observed
 665 by C1. This is made apparent by comparing $(\mathbf{J} \times \mathbf{B}_{C1})_y$ with $(\mathbf{J} \times \mathbf{B}_{AVG})_y$, where the
 666 perturbations are much larger in magnitude for $(\mathbf{J} \times \mathbf{B}_{C1})_y$. We also note that both
 667 $(\mathbf{J} \times \mathbf{B}_{AVG})_y$ and $(\mathbf{J} \times \mathbf{B}_{C1})_y$ are effectively always positive with respect to their model
 668 equivalents. However, $(\mathbf{J} \times \mathbf{B}_{AVG})_y$ is still mostly net negative whereas $(\mathbf{J} \times \mathbf{B}_{C1})_y$ is net
 669 positive. This suggests that using \mathbf{B}_{C1} , rather than \mathbf{B}_{AVG} in calculating $(\mathbf{J} \times \mathbf{B})_y$ has overall

670 reduced the effects of the larger-scale background field curvature (incorporated by
 671 including the other spacecraft). Second, the magnetic field and flow dynamics evident in Fig.
 672 6 appear to almost always be associated with positive (duskward) enhancements in $(\mathbf{J} \times \mathbf{B})_y$,
 673 in contrast to the model dawnward sense of $(\mathbf{J} \times \mathbf{B})_y$. This is particularly evident in the case
 674 of $(\mathbf{J} \times \mathbf{B}_{C1})_y$, but also generally true in the case of $(\mathbf{J} \times \mathbf{B}_{AVG})_y$. We therefore suggest that
 675 the dynamic behaviour of $(\mathbf{J} \times \mathbf{B})_y$ is simply consistent with the localised kinks and flapping
 676 in the magnetic field that are associated with the transient perturbations to the dusk-dawn
 677 flow observed by C1.

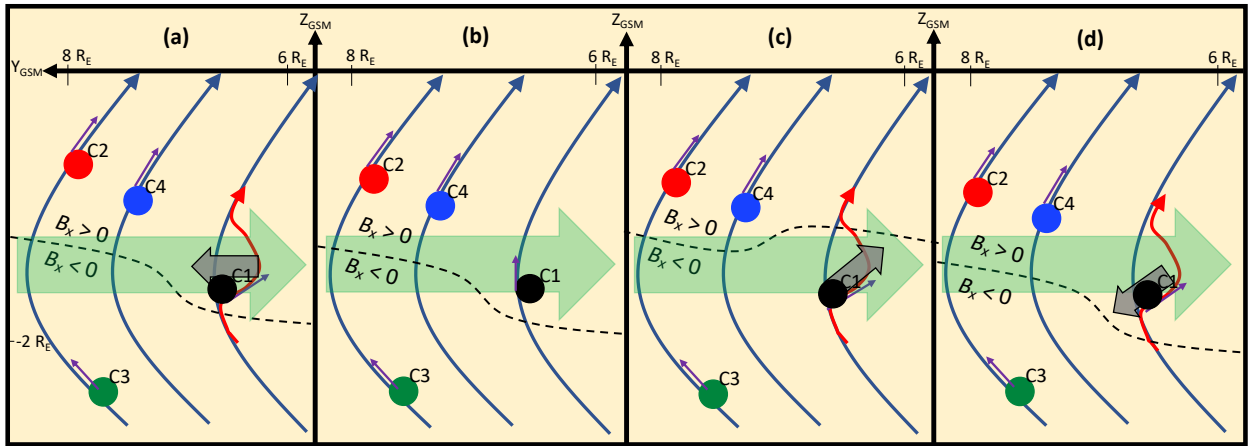
678

679

680 *4.4 Visualization of the observed dynamics*

681 In an effort to visualize these plasma sheet dynamics, we show in Figure 7 a series of
 682 sketches that attempt to associate the observed magnetic field perturbations with the
 683 observed dusk-dawn convective flows. The panels correspond to the four time-windows
 684 indicated on Figure 6 by the highlighted regions labelled a-d. In each panel, we indicate the
 685 approximate relative position of the 4 Cluster spacecraft in GSM coordinates, and the
 686 appropriate sense of B_y measured by each spacecraft is shown by the purple arrows at each
 687 spacecraft location (the Z-component of the field was in fact generally small, and has been
 688 exaggerated here for illustrative purposes). We also superimpose nominal plasma sheet
 689 field lines (again with an exaggerated extent in Z) that display the sense of B_y implied by the
 690 TA15 data presented in Figure 5 (long blue curved arrows). The dashed lines represent the
 691 location of the neutral sheet at the end of each time window. This is tilted slightly, as
 692 appropriate for IMF $B_y > 0$, but with the end-state of the “flap” of the current sheet implied
 693 by the sign of B_x observed by C1. In red is the perturbation to the field implied by the sign of
 694 B_y observed by C1.

695



696

697

698 **Figure 7:** Schematic diagrams of the observed magnetic field perturbations and dusk-dawn

699 convective flows during the time-windows indicated in Fig. 6 by the highlighted regions. The

700 approximate locations of the four Cluster spacecraft relative to one-another in the Y-Z GSM

701 plane are indicated (not to scale) by the coloured circles. The curved blue arrows represent

702 magnetic field lines, and the short purple arrow indicates the local sense of B_y at the

703 location of each spacecraft. The dashed black line indicates the current sheet. In panels (a),

704 (c) and (d), the curved red arrow shows the ‘kinked’ magnetic field line. The long thick green

705 arrow shows the direction of the model $(\mathbf{J} \times \mathbf{B})_y$ force associated with the background

706 curvature of the magnetic field, and the small thick gray arrow shows the direction of the

707 dusk-dawn convective flow observed by C1.

708

709

710 In Fig. 7a C1 is located above the current sheet and measured negative B_y . A weakly

711 duskward convective flow was observed at this time (as indicated by the thick gray arrow),

712 consistent with the duskward sense of the $(\mathbf{J} \times \mathbf{B})_y$ force, and opposite to the sense of the

713 model $(\mathbf{J} \times \mathbf{B})_y$ force associated with the background curvature of the magnetic field. In Fig.

714 7b, C1 is still above the current sheet but measured $B_y \approx 0$ and no dusk-dawn convective

715 flow. In Fig. 7c C1 is shown below the current sheet, where the background B_y would be

716 positive (see Fig. 5b). C1 instead observed an increasingly negative B_y , which we suggest is

717 associated with the presence of the kink in the field. At the same time, C1 also observed a

718 convective plasma flow with downward and slightly upward (+Z) component (thick gray

719 arrow). We therefore suggest that the flow was associated with the upward/dawnward flap
 720 of the current sheet, and that the dawnward sense of the flow likely also resulted in the
 721 increase in negative B_y seen during the time-window shown in Fig. 6c. The positive
 722 $(\mathbf{J} \times \mathbf{B}_{C1})_y$ at this time, whilst inconsistent with the dawnward sense of the flow, is therefore
 723 consistent with the curvature of the magnetic field associated with the kink. $(\mathbf{J} \times \mathbf{B}_{AVG})_y$,
 724 meanwhile, was negative, likely due to incorporating the larger-scale background curvature
 725 of the magnetic field observed by the other spacecraft. In Fig. 7d C1 is shown above the
 726 current sheet, where it observed a weakly negative B_y . In this case, C1 observed a
 727 convective plasma flow with duskward and slightly downward ($-Z$) component. Similarly to
 728 in Fig. 7a, this flow occurred in concert with a positive enhancement in $(\mathbf{J} \times \mathbf{B})_y$ relative to
 729 the model $(\mathbf{J} \times \mathbf{B})_y$. This flow would therefore seem to be associated with the downward
 730 flap of the current sheet, and its duskward sense could indicate that it is acting to reduce
 731 the negative kink in B_y that is apparent over the time-window shown in Fig. 6d.

732

733 Whilst we acknowledge a degree of uncertainty in the details of the interpretation
 734 presented above of the specific relationship between the flows and the field, it serves to
 735 illustrate three observations about this interval of which we can be very certain: 1) The IMF,
 736 ionospheric convection, and comparison of the plasma sheet magnetic field observations to
 737 the TA15 model field, all lead to the expectation of an IMF $B_y > 0$ large-scale asymmetry in
 738 the magnetosphere. 2) The Cluster 1 spacecraft observed convective flow with a dusk-dawn
 739 component that was inconsistent with current theories of IMF B_y -induced dusk-dawn flows
 740 associated with magnetotail untwisting. Notably, the observed dawnward flow in the
 741 southern hemisphere, whilst inconsistent with IMF $B_y > 0$, was also inconsistent with the
 742 expected (symmetric) duskward flow at this pre-midnight location even in the absence of
 743 IMF B_y control. 3) Magnetic field perturbations that were indicative of a localised current
 744 sheet flapping and dusk-dawn kink in the field occurred coincident with the flows. It
 745 therefore seems likely that in this case the IMF B_y -driven asymmetry, or indeed the
 746 symmetric flow expected at the spacecraft location, was being overridden by the localised
 747 dynamics in governing the dusk-dawn component of the flow.

748

749

750 **5. Summary**

751

752 We have presented a case study from 12 October 2006 revealing a dynamic interval of
753 plasma flows and current sheet flapping, observed by the Cluster 1 spacecraft. The key
754 observations presented in this study may be summarised as follows:

755

756 • The OMNI data revealed that the IMF B_y had been positive for several hours prior to
757 our interval of Cluster data, with the exception of three short-lived negative
758 excursions.

759 • The SuperDARN ionospheric convection observations revealed a large-scale
760 asymmetry consistent with IMF $B_y > 0$, confirming the absence of a large-scale
761 asymmetry in the flow pattern that might explain the dawnward flows observed by
762 C1.

763 • C1 observed a changing B_x magnetic field component and associated duskward ($v_{\perp y}$
764 > 0) flow when in the northern magnetic hemisphere, and dawnward ($v_{\perp y} < 0$) flow
765 in the southern magnetic hemisphere.

766 • The C2, C3 and C4 magnetic field observations suggested that the local B_y was being
767 dominated by magnetotail flaring, as opposed to IMF B_y . C3 also observed duskward
768 flow in the southern magnetic hemisphere, consistent with the symmetric flow
769 expected owing to the pre-midnight location of the spacecraft.

770

771 Contrary to the results of a number of previous studies in the literature, during this
772 particular interval, the dusk-dawn sense of the convective magnetotail flows ($v_{\perp y}$); and in
773 particular, the dawnward flow observed in the southern hemisphere, does not agree with
774 expectations based on the theoretical understanding of global magnetotail untwisting and
775 the prevailing positive IMF B_y conditions, nor to expectations based on the location of the
776 spacecraft and associated magnetotail flaring. We instead attribute the flows to a localised
777 magnetic field perturbation, or 'kink' in the magnetotail, which appears to have been
778 independent of any large-scale dynamics and may have instead been related to the
779 observed current sheet flapping. We attributed the current sheet flapping to being driven
780 by localised reconnection, itself inferred from the presence of the observed bursty fast

781 earthward flow ($v_{\perp x} \approx 200 \text{ km s}^{-1}$). Analysis using the curlometer technique suggests that
782 the $(\mathbf{J} \times \mathbf{B})_y$ force is consistent with the localised kinks and flapping in the magnetic field
783 that are associated with the transient perturbations to the dusk-dawn flow observed by C1.

784

785

786 Although evidence for the large-scale penetration of IMF $B_y > 0$ is apparent, the IMF $B_y > 0$
787 penetration at the location of C1 appears to have been unable to override the variable dusk-
788 dawn flow associated with the current sheet flapping. Further studies by the authors are
789 currently underway to determine if such flows are a frequent occurrence, and to consider,
790 and account for, localised tail dynamics more fully in a statistical analysis of the magnetotail
791 flows.

792

793 **Data Availability**

794

795 The sources of data used in this study are included in the acknowledgements section.

796

797

798 **Author Contributions**

799

800 JHL processed the data, performed the data analysis, and drafted the manuscript. AG, NAC
801 and MTW all made substantial and ongoing contributions toward the interpretation and
802 discussion of the observations, in addition to the writing of the manuscript.

803

804

805

806 **Acknowledgements**

807

808 The authors would like to thank the FGM and CIS teams as part of the Cluster mission and
809 acknowledge the Cluster Science Archive (Laakso et al., 2010;
810 <https://www.cosmos.esa.int/web/csa>) as the source of the Cluster data. We also wish to
811 thank the OMNIWeb (<https://omniweb.gsfc.nasa.gov>) as the source of the solar wind and
812 IMF data. The authors acknowledge the use of SuperDARN data. SuperDARN is a collection
813 of radars funded by national scientific funding agencies of Australia, Canada, China, France,
814 Italy, Japan, Norway, South Africa, United Kingdom, and United States of America, and we
815 thank the international PI team for providing the data. The authors acknowledge access to
816 the SuperDARN database via BAS data mirror ([http://bslsuperdarn.ncrc-
817 bas.ac.uk:8093/docs/](http://bslsuperdarn.ncrc-bas.ac.uk:8093/docs/)) and are grateful for use of the Radar Software Toolkit (RST v4.2
818 <https://zenodo.org/record/1403226#.Xy0u7y3MxTY>) with which the raw radar data were
819 processed. We acknowledge the WDC for Geomagnetism, Kyoto, for use of the auroral
820 electrojet indices, which may be obtained from <http://wdc.kugi.kyoto-u.ac.jp/aedir/>. We are
821 also grateful to Haje Korth for providing the IDL Geopack DLM containing the Tsyganenko
822 magnetic field model routines and coordinate system conversions and wish to thank Nikolai

823 Tsyganenko for useful discussion of his magnetic field models. Finally, we are thankful for
824 the advice of Malcolm Dunlop regarding the applicability of the curlometer technique at
825 large spacecraft separations. This research was undertaken with the support of funding
826 from the following sources: Lancaster University Faculty of Science and Technology
827 studentship (JHL), STFC Consolidated grant no. ST/R000816/1 (NAC, AG), NERC standard
828 grant nos. NE/P001556/1 and NE/T000937/1 (MTW, AG). We would also like to thank the
829 two reviewers for their very helpful suggestions which improved the manuscript.

830

831

832 **References**

833

834 Angelopoulos, V., Baumjohann, W., Kennel, C. F., Coroniti, F. V., Kivelson, M. G., Pellat, R.,
835 Walker, R. J., Lühr, H. and Paschmann, G.: Bursty bulk flows in the inner central plasma
836 sheet, *J. Geophys. Res.*, *97 (A4)*, 4027-4039, <https://doi.org/10.1029/91JA02701>, 1992

837

838 Angelopoulos, V., Kennel, C. F., Coroniti, F. V., Pellat, R., Kivelson, M. G., Walker, R. J.,
839 Russell, C. T., Baumjohann, W., Feldman W. C. and Gosling, J. T.: Statistical characteristics of
840 bursty bulk flow events, *J. Geophys. Res.*, *99 (A11)*, 21257-21280,
841 <https://doi.org/10.1029/94JA01263>, 1994

842

843 Balogh, A., Carr, C. M., Acuña, M. H., Dunlop, M. W., Beek, T. J., Brown, P., Fornacon, K. -H.,
844 Georgescu, E., Glassmeier, K. -H., Harris, J., Musmann, G., Oddy, T. and Scwingenschuh, K.:
845 The Cluster magnetic field investigation: Overview of in-flight performance and initial
846 results, *Ann. Geophys.*, *19*, 1207-1217, <https://doi.org/10.5194/angeo-19-1207-2001>, 2001

847

848 Baumjohann, W., Paschmann, G. and Cattell, C. A.: Average Properties in the Central Plasma
849 Sheet, *J. Geophys Res.*, *94 (A6)*, 6597-6606, <https://doi.org/10.1029/JA094iA06p06597>,
850 1989

851

852 Browett, S. D., Fear, R. C., Grocott, A., and Milan, S. E.: Timescales for the penetration of IMF
853 B_y into the Earth's magnetotail, *J. Geophys. Res.: Space Physics*, *122 (1)*, 579-593,
854 <https://doi.org/10.1002/2016JA023198>, 2017

855

856 Cao, J. B., Ma, Y. D., Parks, G., Rème, H., Dandouras, I., Nakamura, R., Zhang, T. L., Zong, Q.,
857 Lucek, E., Carr, C. M., Liu, Z. X. and Zhou, G. C.: Joint observations by Cluster satellites of
858 bursty bulk flows in the magnetotail, *J. Geophys. Res.*, *111 (A4)*, A04206,
859 <https://doi.org/10.1029/2005JA011322>, 2006

860

861 Case, N. A. and Wild, J.: A statistical comparison of solar wind propagation delays derived
862 from multispacecraft techniques, *J. Geophys Res.*, *117 (A2)*, A02101,
863 <https://doi.org/10.1029/2011JA016946>, 2012

864

865 Case, N. A., Grocott, A., Haaland, S., Martin, C. J., and Nagai, T.: Response of the Earth's
866 Neutral Sheet to Reversals in the IMF B_y component, *J. Geophys. Res.*, *123 (10)*, 8206-8218,
867 <https://doi.org/10.1029/2018JA025712>, 2018

868

- 869 Chisham G., Lester, M., Milan, S. E., Freeman, M. P., Bristow, W. A., Grocott A., McWilliams,
870 K. A., Ruohoniemi, J. M., Yeoman, T. K., Dyson, P. L., Greenwald, R. A., Kikuchi, T., Pinnock,
871 M., Rash, J. P. S., Sato, N., Sofko, G. J., Villain, J. -P. and Walker, A. D. M.: A decade of the
872 Super Dual Auroral Radar Network (SuperDARN): scientific achievements, new techniques
873 and future directions, *Surveys in Geophysics* 28, 33-109, [https://doi.org/10.1007/s10712-](https://doi.org/10.1007/s10712-007-9017-8)
874 007-9017-8, 2007
875
- 876 Cowley, S. W. H.: Magnetospheric asymmetries associated with the y-component of the
877 IMF, *Planet Space Sci*, 29 (1), 79-96, [https://doi.org/10.1016/0032-0633\(81\)90141-0](https://doi.org/10.1016/0032-0633(81)90141-0), 1981
878
- 879 Dungey, J. W.: Interplanetary magnetic field and the auroral zones, *Phys. Rev. Lett.*, 6, 47-48,
880 <https://doi.org/10.1103/PhysRevLett.6.47>, 1961
881
- 882 Dunlop, M. W., Southwood, D. J., Glassmeier, K. -H., and Neubauer, F. M.: Analysis of
883 multipoint magnetometer data, *Advances in Space Research*, 8 (9-10), 273-277,
884 [https://doi.org/10.1016/0273-1177\(88\)90141-X](https://doi.org/10.1016/0273-1177(88)90141-X), 1988
885
- 886 Dunlop, M. W., Balogh, A., Glassmeier, K. -H. and Robert, P.: Four-point Cluster application
887 of magnetic field analysis tools: The Curlometer, *J. Geophys. Res.*, 107 (A11),
888 <https://doi.org/10.1029/2001JA005088>, 2002
889
- 890 Escoubet, C. P., Fehringer, M. and Goldstein, M.: The Cluster Mission, *Ann. Geophys.*, 19,
891 1197-1200. <https://doi.org/10.5194/angeo-19-1197-2001>, 2001
892
- 893 Fairfield, D. H.: On the Average Configuration Of The Geomagnetic Tail, *J. Geophys. Res.*, 84
894 (A5), 1950-1958. <https://doi.org/10.1029/JA084iA05p01950>, 1979
895
- 896 Frühauff, D. and Glassmeier, K.-H.: Statistical analysis of magnetotail fast flows and related
897 magnetic disturbances, *Ann. Geophys.*, 34, 399-409, [https://doi.org/10.5194/angeo-34-399-](https://doi.org/10.5194/angeo-34-399-2016)
898 2016, 2016
899
- 900 Grocott, A.: Time Dependence of Dawn-Dusk Asymmetries in the Terrestrial Ionospheric
901 Convection Pattern, In: Haaland, S. et al. (2017), *Dawn-Dusk Asymmetries in Planetary*
902 *Plasma Environments*, John Wiley and Sons, Inc., 107-123, 2017
903
- 904 Grocott, A., Badman, S. V., Cowley, S. W. H, and Cripps, P. J.: The influence of the IMF B_y on
905 the nature of the nightside high-latitude ionospheric flow during intervals of positive IMF B_z .
906 *Ann. Geophys.*, 22, 1755-1764, <https://doi.org/10.5194/angeo-22-1755-2004>, 2004a
907
- 908 Grocott, A., Yeoman, T. K., Cowley, S. W. H, and Rème, H.: Multi-instrument observations of
909 bursty bulk flows and their ionospheric counterparts, *Proc. Seventh Internat. Conf. on*
910 *Substorms*, UDK-52-854, FMI, Helsinki, Finland, 107-110, 2004b
911
- 912 Grocott, A., Yeoman, T. K., Nakamura, R., Cowley, S. W. H, Frey, H. U., Rème, H. and Klecker,
913 B. J.: Multi-instrument observations of the ionospheric counterpart of a bursty bulk flow in
914 the near-Earth plasma sheet, *Ann. Geophys.*, 22, 1061-1075, [https://doi.org/10.5194/angeo-](https://doi.org/10.5194/angeo-22-1061-2004)
915 22-1061-2004, 2004c

- 916
917 Grocott, A., Yeoman, T. K., Milan, S. E. and Cowley, S. W. H.: Interhemispheric observations
918 of the ionospheric signature of tail reconnection during IMF-northward non-substorm
919 intervals, *Ann. Geophys.*, 23, 1763–1770, <https://doi.org/10.5194/angeo-23-1763-2005>,
920 2005
921
922 Grocott, A., Yeoman, T. K., Milan, S. E., Amm, O., Frey, H. U., Juusola, L., Nakamura, R.,
923 Owen, C. J., Rème, H. and Takada, T.: Multi-scale observations of magnetotail flux transport
924 during IMF-northward non-substorm intervals, *Ann. Geophys.*, 25, 1709-1720,
925 <https://doi.org/10.5194/angeo-25-1709-2007>, 2007
926
927 Grocott, A., Milan, S. E. and Yeoman, T. K.: Interplanetary magnetic field control of fast
928 azimuthal flows in the nightside high-latitude ionosphere, *Geophys. Res. Lett.*, 35, L08102,
929 <https://doi.org/10.1029/2008GL033545>, 2008
930
931 Haaland, S., Runov, A. and Forsyth, C.: Dawn-Dusk Asymmetries in Planetary Plasma
932 Environments, *Geophysical Monograph 230, First Edition. American Geophysical Union.*
933 Published 2017 by John Wiley & Sons, Inc., 2017
934
935 Karlsson, T., Hamrin, M., Nilsson, H., Kullen, A., and Pitkänen, T.: Magnetic forces associated
936 with bursty bulk flows in the Earth's magnetotail, *Geophys. Res. Lett.*, 42 (9), 3122-3128,
937 <https://doi.org/10.1002/2015GL063999>, 2015
938
939 Kiehas, S. A., Runov, A., Angelopoulos, V., Hietala, H. and Korovinskiy, D.: Magnetotail Fast
940 Flow Occurrence Rate and Dawn-Dusk Asymmetry at $X_{GSM} \sim -60 R_E$, *J. Geophys. Res.: Space*
941 *Physics*, 123 (3), 1767-1778, <https://doi.org/10.1002/2017JA024776>, 2018
942
943 King, J. H., and Papitashvili, N. E.: Solar wind spatial scales in and comparisons of hourly
944 Wind and ACE plasma and magnetic field data, *J. Geophys. Res.*, 110, A02104,
945 <https://doi.org/10.1029/2004JA010649>, 2005
946
947 Kissinger, J., McPherron, R. L., Hsu, T. -S. and Angelopoulos, V.: Diversion of plasma due to
948 high pressure in the inner magnetosphere during steady magnetospheric convection, *J.*
949 *Geophys. Res.*, 117, A05206, <https://doi.org/10.1029/2012JA017579>, 2012
950
951 Khurana, K. K., Walker, R. J., and Ogino, T.: Magnetospheric convection in the presence of
952 interplanetary magnetic field By: A conceptual model and simulations. *J. Geophys. Res.*, 101
953 (A3), 4907-4916, <https://doi.org/10.1029/95JA03673>, 1996
954
955 Kubyshkina, D. I., Sormakov, D. A., Sergeev, V. A., Semenov, V. S., Erkaev, N. V., Kubyshkin, I.
956 V., Ganushkina, N. Yu. And Dubyagin, S. V.: How to distinguish between kink and sausage
957 modes in flapping oscillations?, *J. Geophys. Res.*, 119, 3002-3015,
958 <https://doi.org/10.1002/2013JA019477>, 2014
959
960 Laakso, H., Perry, C., McCaffrey, S., Herment, D., Allen, D. J., Harvey, C. C., Escoubet, C. P.,
961 Gruenberger, C., Taylor, M. G. G. T. and Turner, R.: Cluster Active Archive: Overview, 3-37,

- 962 The Cluster Active Archive, Astrophysics and Space Science Proceedings, H. Laakso et al.
963 (eds.), Springer, 2010
964
- 965 Lockwood, M.: Modelling high-latitude ionosphere for time-varying plasma convection. IEE
966 Proceedings-H, Vol. 140. No. 2, <https://doi.org/10.1049/ip-h-2.1993.0015>, 1993
967
- 968 Malova, H. V., Zelenyi, L. M., Popov, V. Y., Petrukovich, A. A. and Runov, A. V.: Asymmetric
969 thin current sheets in the Earth's magnetotail, *Geophys. Res. Lett.*, *34* (16), L16108,
970 <https://doi.org/10.1029/2007GL030011>, 2007
971
- 972 McPherron, R. L., Hsu, T. -S., Kissinger, J., Chu, X., and Angelopoulos, V.: Characteristics of
973 plasma flows at the inner edge of the plasma sheet, *J. Geophys. Res.*, *116* (A5), A00133,
974 <https://doi.org/10.1029/2010JA015923>, 2011
975
- 976 Nakamura, R., Baumjohann, W., Klecker, B., Bogdanova, Y., Balogh, A., Rème, H., Bosqued, J.
977 M., Dandouras, I., Sauvaud, J. A., Glassmeier, K. -H., Kistler, L., Mouikis, C., Zhang, T. L.,
978 Eichelberger, H. and Runov, A.: Motion of the dipolarization front during a flow burst event
979 observed by Cluster, *Geophys. Res. Lett.*, *29* (20), 1942,
980 <https://doi.org/10.1029/2002GL015763>, 2002
981
- 982 Nakamura, R., Retinò, A., Baumjohann, W., Volwerk, M., Erkaev, N., Klecker, B., Lucek, E. A.,
983 Dandouras, I., André, M. and Khotyainstev, Y.: Evolution of dipolarization in the near-Earth
984 current sheet induced by Earthward rapid flux transport, *Ann. Geophys.*, *27*, 1743-1754,
985 <https://doi.org/10.5194/angeo-27-1743-2009>, 2009
986
- 987 Ness, N. F.: The Earth's Magnetic Tail. *J. Geophys. Res.*, *70* (13), 2,989-3,005,
988 <https://doi.org/10.1029/JZ070i013p02989>, 1965
989
- 990 Newell, P. T., Sotirelis, T., Liou, K., Meng, C. -I. and Rich, F. J.: A nearly universal solar wind-
991 magnetosphere coupling function inferred from 10 magnetospheric state variables., *J.*
992 *Geophys. Res.*, *112* (A1), A01206, <https://doi.org/10.1029/2006JA012025>, 2007
993
- 994 Nishitani, N., Ruohoniemi, J. M., Lester, M., Baker, J. B. H., Koustov, A. V., Shepherd, S. G.,
995 Chisham, G., Hori, T., Thomas, E. G., Makarevich, R. A., Marchaudon, A., Ponomarenko, P.,
996 Wild, J. A., Milan, S. E., Bristow, W. A., Devlin, J., Miller, E., Greenwald, R. A., Ogawa, T. and
997 Kikiuchi, T.: Review of the accomplishments of mid-latitude Super Dual Auroral Radar
998 Network (SuperDARN) HF radars, *Progress in Earth and Planetary Science*, *6*:27,
999 <https://doi.org/10.1186/s40645-019-0270-5>, 2019
1000
- 1001 Ohma, A., Østgaard, N., Reistad, J. P., Tenfjord, P., Laundal, K. M., Moretto Jørgensen, T.,
1002 Haaland, S. E., Krcelic, P. and Milan, S.: Observations of Asymmetric Lobe Convection for
1003 Weak and Strong Tail Activity, *J. Geophys. Res.: Space Physics*, *124* (12),
1004 <https://doi.org/10.1029/2019JA026773>, 2019
1005
- 1006 Pettigrew, E. D., Shepherd, S. G. and Ruohoniemi, J. M.: Climatological patterns of high-
1007 latitude convection in the Northern and Southern hemispheres: Dipole tilt dependencies

- 1008 and interhemispheric comparisons, *J. Geophys. Res.*, *115*, [https://doi.org/](https://doi.org/10.1029/2009JA014956)
1009 10.1029/2009JA014956, 2010
1010
- 1011 Petrukovich, A. A.: Origins of plasma sheet B_y , *J. Geophys. Res.*, *116* (A7), A07217,
1012 <https://doi.org/10.1029/2010JA016386>, 2011
1013
- 1014 Petrukovich, A. A., Baumjohann, W., Nakamura, R., Schödel, R., and Mukai, T.: Are
1015 earthward bursty bulk flows convective or field-aligned?, *J. Geophys. Res.*, *106* (A10), 21211-
1016 21215, <https://doi.org/10.1029/2001JA900019>, 2001
1017
- 1018 Petrukovich, A. A., Baumjohann, W., Nakamura, R., Runov, A., and Balogh, A.: Cluster vision
1019 of the magnetotail current sheet on a macroscale, *J. Geophys. Res.*, *110* (A6), A06204,
1020 <https://doi.org/10.1029/2004JA010825>, 2005
1021
- 1022 Pitkänen, T., Hamrin, M., Norqvist, P., Karlsson, T., and Nilsson, H.: IMF dependence of the
1023 azimuthal direction of earthward magnetotail fast flows, *Geophys. Res. Lett.*, *40* (21), 5598-
1024 5604, <https://doi.org/10.1002/2013GL058136>, 2013
1025
- 1026 Pitkänen, T., Hamrin, M., Norqvist, P., Karlsson, T., Nilsson, H., Kullen, A., Imber, S. M. and
1027 Milan, S. E.: Azimuthal velocity shear within an earthward fast flow: further evidence for
1028 magnetotail untwisting?, *Ann. Geophys.*, *33*, 245-255., [https://doi.org/10.5194/angeo-33-](https://doi.org/10.5194/angeo-33-245-2015)
1029 245-2015, 2015
1030
- 1031 Pitkänen, T., Hamrin, M., Karlsson, T., Nilsson, H., and Kullen, A.: On IMF B_y -Induced Dawn-
1032 Dusk Asymmetries in Earthward Convective Fast Flows, In: Haaland, S. et al. (2017), *Dawn-*
1033 *Dusk Asymmetries in Planetary Plasma Environments*, John Wiley and Sons, Inc., 107-123,
1034 2017
1035
- 1036 Pitkänen, T., Kullen, A., Laundal, K. M., Tenfjord, P., Shi, Q. Q. Park. J. -S., Hamrin, M., De
1037 Spiegeleer, A., Chong, G. S. and Tian, A. M.: IMF B_y Influence on Magnetospheric Convection
1038 in Earth's Magnetotail Plasma Sheet, *Geophys. Res. Lett.*, *46* (21), 11698-11708,
1039 <https://doi.org/10.1029/2019GL084190>, 2019
1040
- 1041 Reistad, J. P., Østgaard, N., Tenfjord, P., Laundal, K. M., Snekvik, K., Haaland, S., Milan, S. E.,
1042 Oksavik, K., Frey, H. U. and Grocott, A.: Dynamic effects of restoring footprint symmetry on
1043 closed magnetic field lines, *J. Geophys. Res.: Space Physics*, *121* (5), 015JA022058,
1044 <https://doi.org/10.1002/2015JA022058>, 2016
1045
- 1046 Reistad, J. P., Østgaard, N., Laundal, K. M., Ohma, A., Snekvik, K., Tenfjord, P., Grocott, A.,
1047 Oksavik, K., Milan, S. E. and Haaland, S.: Observations of asymmetries in ionospheric return
1048 flow during different levels of geomagnetic activity, *J. Geophys. Res.*, *123*,
1049 <https://doi.org/10.1029/2017JA025051>, 2018
1050
- 1051 Rème, H., Bosqued, J. M., Sauvaud, J. A., Cros, A., Dandouras, J., Aoustin, C., Bouyssou, J.,
1052 Camus, Th., Cuvilo, J., Martz, C., Médale, J. L., Perrier, H., Romefort, D., Rouzaud, J., d'Uston,
1053 C., Möbius, E., Crocker, K., Granoff, M., Kistler, L. M., Popecki, M., Hovestadt, D., Klecker, B.,
1054 Paschmann, G., Scholer, M., Carlson, C. W., Curtis, D. W., Lin, R. P., McFadden, J. P.,

- 1055 Formisano, V., Amata, E., Bavassano-Cattaneo, M. B., Baldetti, P., Belluci, G., Bruno, R.,
1056 Chionchio, G., Di Lellis, A., Shelley, E. G., Ghielmetti, A. G., Lennartsson, W., Korth, A.,
1057 Rosenbauer, H., Lundin, R., Olsen, S., Parks, G. K., McCarthy, M. and Balsiger, H.: The Cluster
1058 Ion Spectrometry (CIS) Experiment, *Space Sci. Rev.*, *79*, 303-350,
1059 https://doi.org/10.1007/978-94-011-5666-0_12, 1997
1060
1061 Rong, Z. J., Barabash, S., Stenberg, G., Futaana, Y., Zhang, T. L., Wan, W. X., Wei, Y. and
1062 Wang, X. -D.: Technique for diagnosing the flapping motion of magnetotail current sheets
1063 based on single-point magnetic field analysis, *J. Geophys. Res.: Space Physics*, *120* (5), 3462-
1064 3474, <https://doi.org/10.1002/2014JA020973>, 2015
1065
1066 Runov, A. Nakamura, R., Baumjohann, W., Zhang, T. L., Volwerk, M., Eichelberger, H. -U. and
1067 Balogh, A.: Cluster observations of a bifurcated current sheet, *Geophys. Res. Lett.*, *30* (2),
1068 1036, <https://doi.org/10.1029/2002GL016136>, 2003
1069
1070 Runov, A., Angelopoulos, V., Sergeev, V. A., Glassmeier, K. -H., Auster, U., McFadden, J.,
1071 Larson, D. and Mann, I.: Global properties of magnetotail current sheet flapping: THEMIS
1072 perspectives, *Ann. Geophys.*, *27*, 319-328, <https://doi.org/10.5194/angeo-27-319-2009>,
1073 2009
1074
1075 Ruohoniemi, J. M. and Baker, K. B.: Large-scale imaging of high-latitude convection with
1076 Super Dual Auroral Radar Network HF radar observations, *J. Geophys. Res.*, *103* (A9), 20797-
1077 20811, <https://doi.org/10.1029/98JA01288>, 1998
1078
1079 Ruohoniemi, J. M. and Greenwald, R. A.: Statistical patterns of high-latitude convection
1080 obtained from Goose Bay HF radar observations, *J. Geophys. Res.*, *101* (A10), 21743-21763,
1081 <https://doi.org/10.1029/96JA01584>, 1996
1082
1083 Sergeev, V. A., Angelopoulos, V., Gosling, J. T., Cattell, C. A., and Russell, C. T.: Detection of
1084 localised, plasma-depleted flux tubes or bubbles in the midtail plasma sheet, *J. Geophys.*
1085 *Res.*, *101* (A5), 10817 – 10826, <https://doi.org/10.1029/96JA00460>, 1996
1086
1087 Sonnerup, B. U. Ö, and Cahill Jr, L. J.: Magnetopause structure and attitude from Explorer 12
1088 observations, *J. Geophys. Res.*, *72* (1), 171-183, <https://doi.org/10.1029/JZ072i001p00171>,
1089 1967
1090
1091 Sonnerup, B. U. Ö and Scheible, M.: Minimum and Maximum Variance Analysis, In:
1092 Paschmann, G. and Daly, W. (1998), *Analysis Methods for Multi-Spacecraft Data*, pp 185-
1093 220, ESA Publications Division, Noordwijk, Netherlands, 1998
1094
1095 Tenfjord, P., Østgaard, N., Snekvik, K., Laundal, K. M., Reistad, J. P., Haaland, S., and Milan, S.
1096 E.: How the IMF B_y induces a B_y component in the closed magnetosphere and how it leads to
1097 asymmetric currents and convection patterns in the two hemispheres, *J. Geophys. Res.:*
1098 *Space Physics*, *120* (11), 9368-9384, <https://doi.org/10.1002/2015JA021579>, 2015
1099

- 1100 Tenfjord, P., Østgaard, N., Strangeway, R., Haaland, S., Snekvik, K., Laundal, K. M., Reistad, J.
1101 P. and Milan, S. E.: Magnetospheric response and reconfiguration times following IMF By
1102 reversals, *J. Geophys. Res.: Space Physics*, *122* (1), 417-431,
1103 <https://doi.org/10.1002/2016JA023018>, 2017
1104
- 1105 Thomas, E. G. and Shepherd, S. G.: Statistical Patterns of Ionospheric Convection Derived
1106 From Mid-Latitude, High-Latitude and Polar SuperDARN HF Observations, *J. Geophys. Res.:*
1107 *Space Physics*, *123* (4), 3196-3216, <https://doi.org/10.1002/2018JA025280>, 2017
1108
- 1109 Tsyganenko, N. A. and Andreeva, V. A.: A forecasting model of the magnetosphere driven by
1110 an optimal solar wind coupling function, *J. Geophys. Res.*, *120* (10), 8401-8425,
1111 <https://doi.org/10.1002/2015JA021641>, 2015
1112
- 1113 Volwerk, M., Zhang, T. L., Glassmeier, K. -H., Runov, A., Baumjohann, W., Balogh, A., Rème,
1114 H., Klecker, B. and Carr, C.: Study of waves in the magnetotail region with cluster and DSP,
1115 *Advances in Space Research*, *41* (10), 1593-1597, <https://doi.org/10.1016/j.asr.2007.04.005>,
1116 2008
1117
- 1118 Wei, X. H., Cai, C. L., Cao, J. B., Rème, H., Dandouras, I., and Parks, G. K.: Flapping motions of
1119 the magnetotail current sheet excited by nonadiabatic ions, *Geophys. Res. Lett.*, *42*, 4731-
1120 4735, <https://doi.org/10.1002/2015GL064459>, 2015
1121
- 1122 Wei, Y. Y., Huang, S. Y., Rong, Z. J., Yuan, Z. G., Jiang, K., Deng, X. H., Zhou, M., Fu, H. S., Yu,
1123 X. D., Xu, S. B., He, L. H. and Deng, D.: Observations of Short-period Current Sheet Flapping
1124 Events in the Earth's Magnetotail, *The Astrophysical Journal Letters*, *874*, 7pp.
1125 <https://doi.org/10.3847/2041-8213/ab0f28>, 2019
1126
- 1127 Wu, M., Lu, Q., Volwerk, M., Vörös, Z., Ma, X., and Wang, S.: Current sheet flapping motions
1128 in the tailward flow of magnetic reconnection, *J. Geophys. Res.*, *121* (8), 7817-7827,
1129 <https://doi.org/10.1002/2016JA022819>, 2016
1130
- 1131 Zhang, L. Q., Baumjohann, W., Wang, C., Dai, L., and Tang, B. B.: Bursty bulk flows at
1132 different magnetospheric activity levels: Dependence of IMF conditions, *J. Geophys. Res.*,
1133 *121* (9), 8773-8789, <https://doi.org/10.1002/2016JA022397>, 2016
1134
1135